Microsyst Technol (2010) 16:117–141
DOI 10.1007/s00542-008-0772-3

TECHNICAL PAPER

Precision positioning of a three-axis optical pickup via a double phase-lead compensator equipped with auto-tuned parameters

Paul C.-P. Chao · Chi-Wei Chiu · Jackal C.-Y. Shen

Received: 3 August 2008 / Accepted: 10 December 2008 / Published online: 31 January 2009

Abstract The objective of this study is to design an intelligent control servo scheme for the three-axis optical pickups employed in the next-generation optical disc drives. The three-axis pickup owns the capability to move the lens holder in three directions of focusing, tracking and tilting, which is required particularly for higher data-density optical disks and precision measuring instruments to annihilate non-zero lens tilting. The intelligent controller utilizes a commercially often-used double phase-lead compensator equipped with the capability of auto-tuning on control parameters. In this way, the model uncertainty of the pickups caused by manufacturing tolerance and the coupling between three different DOFs of the three-axis pickup can be overcome to render desired precision data-reading. In the initial stage of the study, Lagrange's equations are employed to derive equations of motion for the lens holder. A double-lead controller equipped with a fuzzy logic parameter tuning algorithm is then designed to perform dynamic decoupling and forge control efforts toward the goals of precision tracking, focusing and zero tilting simultaneously. Along with the controller, a genetic algorithm is developed to search the optimal designed parameters of previously designed auto-tuning algorithm. Finally, the experiments are conducted to show the effectiveness of the controller. With validated performance, the designed intelligent controller is ready to be employed for the next-generation optical disc drives.

P. C.-P. Chao (✉) · C.-W. Chiu
Department of Electrical and Control Engineering,
National Chiao Tung University, Hsinchu 300, Taiwan
e-mail: pchao@mail.nctu.edu.tw

J. C.-Y. Shen
Department of Mechanical Engineering,
Chung-Yuan Christian University, Chung-Li 320, Taiwan

1 Introduction

For optical disk drives (ODDs) and some surface-profiling instruments in micro- or nano-precisions (Zhang and Cai 1997; Fan et al. 2000, 2001), the key component determining the performance is the optical pickup, which conducts data-reading via a well-designed optical system installed inside the pickup. Figure 1 shows a photo of a three-axis four-wire type pickup actuator, which is designed and manufactured by the Industrial Technology and Research Institute (ITRI), Taiwan. This pickup consists mainly of an objective lens, a lens holder (often called "bobbin"), wire springs, sets of wound coils and permanent magnets. Thanks to flexibility of wire springs, the bobbin could easily be in motions as the forces acting on the bobbin are generated by the electromagnetic interactions between the magnetic fields induced by permanent magnets and the currents conducted in sets of coils.

High-numerical apertures (NA) and short-wavelength laser diode (like violet diodes) are recently employed for objective lens designs in pickups in order to produce a smaller optical detecting spot on an optical disk for better data-reading resolution. This aims at increasing detectable data-density via decreasing the circular radius of the aberration region of the optical spot, the main factor limiting resolution of data storage in disks for ODDs or surface profiling for measuring instruments. With the size of optical spot decreased, original electro-mechanical designs of the pickup structure might become obsolete. One of critical challenges arises from the unavoidable

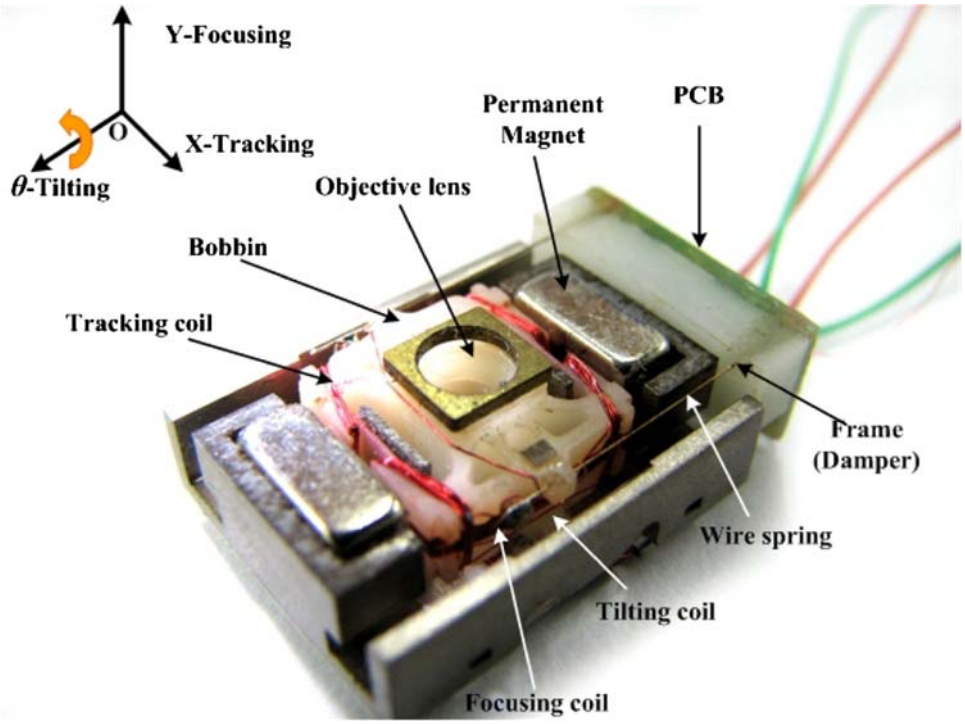

Fig. 1 Structure of the three-axis four-wire type optical pickup by ITRI

tilting of the bobbin during its motion since the resulted coma aberration increases in proportion to NA^3/λ, where λ is the wavelength of the laser diode (Nagasato and Hoshino 1996). This tilting arises from two possible factors. The first factor is an uneven magnetic field due to manufacturing tolerance and/or the mis-pass of the net electromagnetic force in the directions of focusing and tracking to the mass center of the bobbin while the bobbin moves from its static position to desired vertical and radial positions. This factor leads to a tilting moment on the bobbin and then a nonzero bobbin tilt. The second factor is the unavoidable small un-parallelism in practice between the lens and the optical disc in high-speed rotations or the surface to profile. To restrain the bobbin tilting to a small level for a more accurate, faster data-reading, some research works (Choi et al. 2001; Kang and Yoon 1998; Rosmalen 1987; Yamada et al. 2000; Chao et al. 2003; He et al. 2004) have successfully developed the tilt servo systems for the bobbin, in addition to original focusing and tacking ones. The tilt servo makes possible the capability of suppressing the unavoidable bobbin tiltings. One of challenges for implementation, however, arises from the manufacturing tolerance existing in each commercial four-wire type pickup, which makes uncertain if the afore-designed controllers still works in the presence of tolerance and the dynamic coupling between three axes of the pickup. Table 1 lists dynamic characteristics of four-four-wire type optical pickups of the same model no. and their variations tested in the laboratory. It is clear that the dynamics of the pickups are not the same to each other, and thus a controller designed based on one single pickup is not guaranteed to also work for others.

To solve above-mentioned problem, the available intelligent servo methods for the next-generation servo to perform precision positioning is developed in this study. The design concept of this intelligent control servo system relies on tuning the control parameters automatically using some intelligent frameworks. We use the well-known fuzzy logic controller (FLC) to change the parameters in double phase-lead compensators to save the response time and

Table 1 Specifications of two difference four-wire type optical pickups

Difference optical pickup	Focusing		Tracking		Tilting	
	No. 1	No. 2	No. 1	No. 2	No. 1	No. 2
Resonance frequency (Hz)	53.3	54.5	77.68	79.22	145.86	143.62
Resonance peak (dB)	59.181	60.21	59.99	61.56	48.7	47.66
Magnitude (dB)	52.3	53.1	51.35	50.33	46.2	38.3
Phase angle in 1,000 Hz (°)	−179.77	−178.56	−179.89	−178.6	−179.9	−178.4

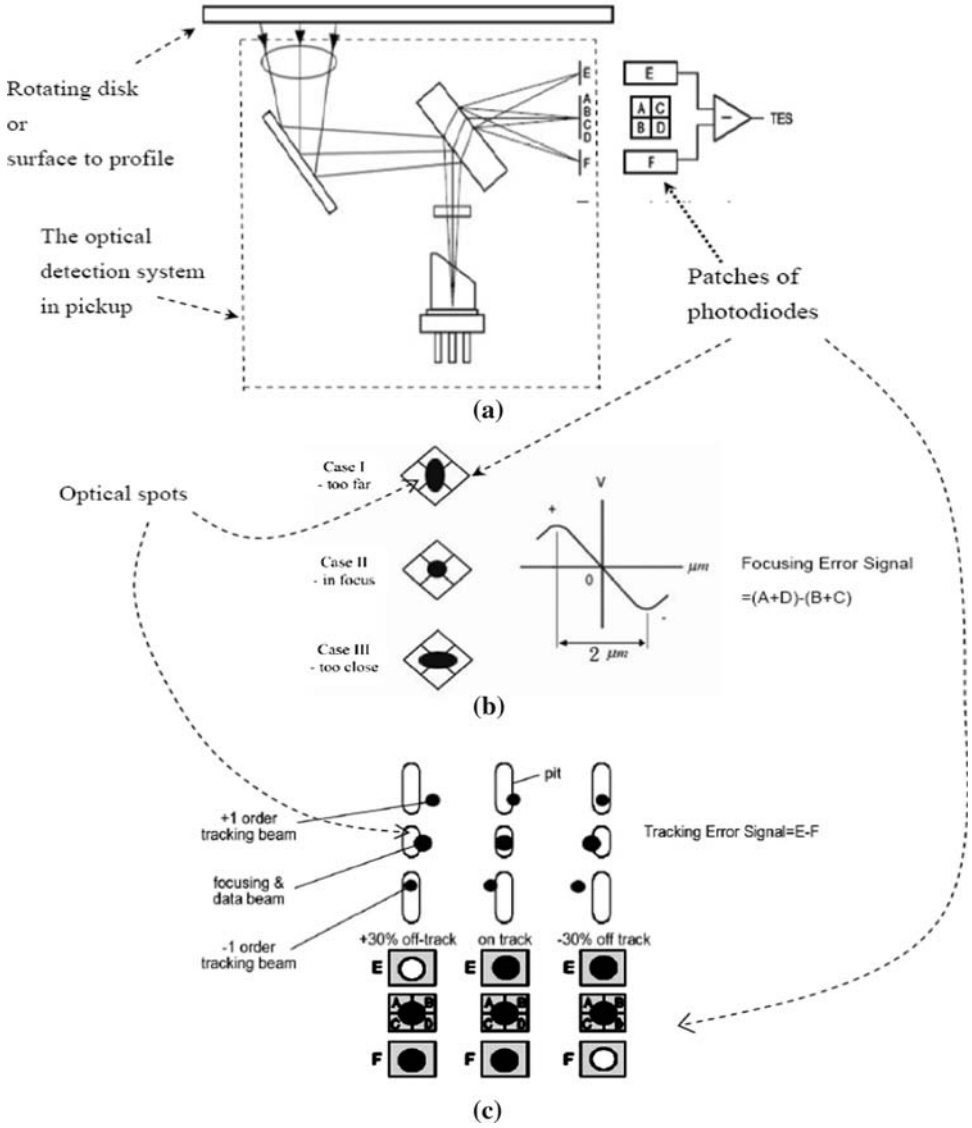

Fig. 2 **a** The optical system of the pickup including photodiodes, **b** The method of quad-detectors measuring focusing error, **c** The three-beam method for measuring tracking error

attain better performance of controller. In addition, the membership functions are searched by genetic algorithm (GA) to perform dynamic decoupling and forge control efforts toward the goals of precision tracking, focusing and zero tilting. In Akgül and Morgül (1997), Hong et al. (1992), Visioli (1999), and Hsu and Tsai (1996), the studies describe the tunings on the parameters of the PID or lead–lag controller by FLC designs for improving the system responses. From above studies, the main advantage of the FLC is its inherent robustness and ability to handle any nonlinear behavior of the structure. Another advantage is that engineers can design a FLC easily because the principle of a FLC is simple to understand. Therefore, the parameter of the double-lead compensator is tuned by FLC in this study. However, there are some parameters needed to be searched in the FLC for attaining better performance. GA is chosen herein for searching for optimal memberships and associated peak gains in the FLC. In Hwang and Thompson (1994), a similar GA is presented for the FLC. The domains of the membership functions of the FLC are searched. It is pertinent to note at this point that the intelligent servo in practice for this study needs to acquire on-line feedbacks of bobbin motions not only in DOFs of focusing and tracking but also tilting. For conventional pickups, only motions of tracking and focusing can be detected by specifically designed optical systems and several patches of photo-detectors (Marchant 1990). Figure 2 illustrates a typical optical/sensing system for measuring the motions of the bobbin, where Fig. 2a presenting the overall optical system, Fig. 2b showing the principle of quad-detectors for detecting focusing motions, while Fig. 2c the three-beam method for tracking motions. It is can easily be seen from Fig. 2 that the conventional optical system needs additional patches of photo-detectors or apply the recently proposed methods of signal analysis (Katayama et al. 2001; Miyano and Nagara 2004;

Yamasaki et al. 2006) on the reflected light intensity to equip itself with the capability of tilt detection.

In the next section, the mathematical modeling for the optical pickup will be presented. In Sect. 3 the double-lead compensator and auto-tuning algorithm are designed. Numerical and experimental results are subsequently presented in Sects. 4 and 5, respectively. Finally conclusions and future works are stated in Sect. 6.

2 Mathematical modeling

A typical three-axis pickup actuator designed fabricated by ITRI, as shown in Fig. 1, is considered in this study. This pickup mainly consists of a lens holder—bobbin, inner/outer yokes, four-wire springs, coils for actuations in directions of tracking/focusing/tilting, four permanent magnets and a PCB holder. To actuate the pickup, three external voltages are applied independently across the respective spring wires to generate the wire-carried currents through the magnetic fields posed by surrounding magnets. It generates independent actuation forces and moments to perform simultaneous by positioning and rotating in the directions of focusing/tracking and tilting, respectively. According to (Chao et al. 2003), the mathematical modeling of three-axis pickup was established accurately as following section.

2.1 Dynamic modeling of actuator

The conventional bobbin, due to its specially designed supporting structure of four parallel wires, exhibits motions mainly in the DOFs of tracking (X-axis) and focusing (Y-axis). In addition to the motions in X and Y directions, small tilting often occurs about θ-axis, which is caused by manufacturing tolerance, uneven magnetic fields, and/or geometric mis-passes of the electro-magnetic forces acting line on the bobbin mass center. The objective of this study is to design a fuzzy controller that owns three independent actuating forces and moment in X, Y and θ directions in order to perform precision focusing/tracking and to simultaneously achieve zero tilting to avoid any errors in optical reading signals. The design of such controller starts with an establishment of the system dynamic model. It is assumed that the pickup assembly can be simply modeled as a lumped mass-spring-damper system due to bobbin's high material rigidity compared to the flexibility of the suspending wires. Figure 3 shows the schematic on the bobbin from the planar side view of Fig. 1 (from the viewpoint toward the X–Y plane), and accompanying coordinates/notations defined for capturing the bobbin motion. As seen in Figs. 1 and 3 are coordinates xyz defined as the body-fixed ones to the moving bobbin, while

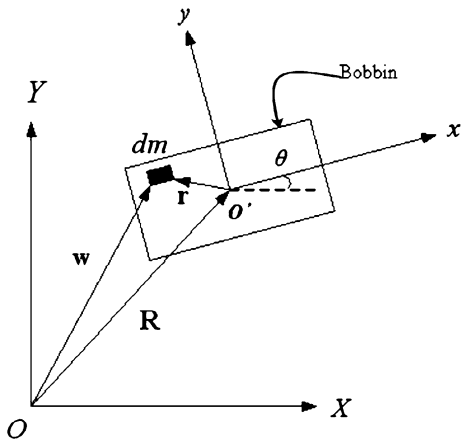

Fig. 3 Planar dynamic model of the bobbin from side view in Fig. 1

coordinates XYZ are global, ground coordinates. X also serves as a dynamic variable, capturing the horizontal, tracking motion; Y does the vertical, focusing motion; θ does the rotating angle of the bobbin about Z; i.e., the tilting angle. The displacement vector w for a given point of the bobbin can be represented by

$$\mathbf{w} = \mathbf{R} + \mathbf{Tr} \tag{1}$$

where $\mathbf{R} = [X\ Y\ O]^T$ is the position vector of bobbin centroid, O, measured from the origin of the ground coordinates XYZ, O. Also,

$$\mathbf{T} = \begin{bmatrix} \cos\theta & -\sin\theta & 0 \\ \sin\theta & \cos\theta & 0 \\ 0 & 0 & 1 \end{bmatrix}$$

is the transformation matrix due to θ, and $\mathbf{r} = [X\ Y\ O]$ is the position vector of a differential mass dm in the bobbin as shown in Fig. 3. Differentiating Eq. 1 with respect to time and putting into kinetic energy, the kinetic energy of the bobbin can be obtained as

$$\begin{aligned} L_T &= \frac{1}{2}\int_m \dot{\mathbf{w}}^T \dot{\mathbf{w}} dm \\ &= \frac{1}{2}m\left(\dot{X}^2 + \dot{Y}^2\right) + \frac{1}{2}I_\theta\dot{\theta}^2 - \dot{X}\dot{\theta}\left(I_x\sin\theta + I_y\cos\theta\right) \\ &\quad + \dot{Y}\dot{\theta}\left(I_x\cos\theta - I_y\sin\theta\right), \end{aligned} \tag{2}$$

where I_θ is the mass moment of inertia of the bobbin about its centroid along z-axis, while $I_x = \int_m x dm$ and $I_y = \int_m y dm$ are first mass moments of inertia with respect to x and y axes, respectively. The potential energy of the pickup is next expressed as

$$V = \frac{1}{2}\left(k_x X^2 + k_y Y^2 + k_\theta\theta^2\right) + mgY, \tag{3}$$

where k_x, k_y and k_θ are the equivalent spring stiffnesses in tracking, focusing and tilting directions; m is the mass of

bobbin; g is the gravitation. Finally, the non-conservative virtual work can be derived as

$$\delta W = \int_A (\mathbf{T}\cdot\mathbf{F})^T \delta \mathbf{w} dA$$
$$= \big(F_x\cos\theta - F_y\sin\theta\big)\delta X + \big(F_x\sin\theta + F_y\cos\theta\big)\delta Y + F_\theta \delta\theta, \quad (4)$$

where δW enotes virtual work while, F_x and F_y represent the actuation forces acting on the centroid, respectively, in the tracking and focusing directions. F_θ denotes the torsional moment about θ. δW is the virtual bobbin displacement due to the applied force F. Substituting Eqs. 2–4 into Lagrange's equation (Meirovitch 1967), the equations of motion can be readily obtained as

$$M\ddot{\mathbf{q}} + \mathbf{K}\mathbf{q} + \mathbf{N} + \mathbf{G} = \mathbf{T}\mathbf{F}, \quad (5)$$

where $\mathbf{q} = [X\ Y\ \theta]^T$ contains the generalized coordinates for describing the motion of the bobbin. **M** and **K** are overall mass and stiffness matrices. **N** contains the centrifugal and Coriolis force terms. **G** captures the gravitational effect. **F** captures the actuator forces. Their expressions are given in the followings,

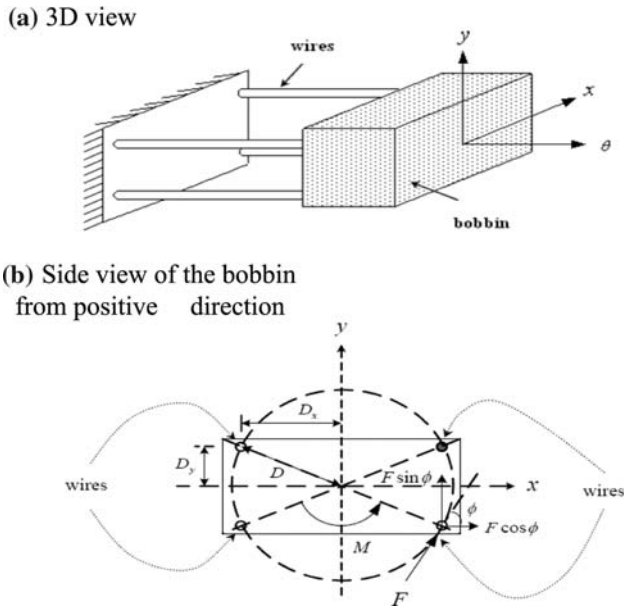

Fig. 4 Moment generation of the four-wire-type optical pickup

$$\mathbf{M} = \begin{bmatrix} m & 0 & -\big(I_x\sin\theta + I_y\cos\theta\big) \\ 0 & m & \big(I_x\cos\theta - I_y\sin\theta\big) \\ -\big(I_x\sin\theta + I_y\cos\theta\big) & \big(I_x\cos\theta - I_y\sin\theta\big) & I_\theta \end{bmatrix},$$

$$\mathrm{K}_0 = \mathrm{diag}\big[k_x,\ k_y,\ k_\theta\big] \quad \mathbf{F} = [F_X \quad F_Y \quad F_\theta]^T, \mathbf{G} = [0 \quad mg \quad 0]^T,$$

$$\mathbf{N} = \begin{bmatrix} -\dot\theta^2\big(I_x\cos\theta - I_y\sin\theta\big) \\ -\dot\theta^2\big(I_x\sin\theta + I_y\cos\theta\big) \\ \dot X\dot\theta\big(I_x\cos\theta - I_y\sin\theta\big) + \dot Y\dot\theta\big(I_x\sin\theta + I_y\cos\theta\big) \end{bmatrix}.$$

The stiffness coefficients in the above $\mathbf{K}_0$, $(k_x,\ k_y)$ comply with

$$k_x = k_y = 4\cdot\frac{12EI_w}{L^3}, \quad (6)$$

where E is the elastic modulus, I_w is the area moment of inertia about x- or y-axis for the wire, and L is the length of each wire. The expression of k_θ is next due to be derived. To this end, Fig. 4 are first depicted to illustrate how to derive the moment M responsible for the tilting of the bobbin. In Fig. 4, F represents the combined electro-magnetic force in focusing and tracking directions, which is generated by the current carried by a wire at some instant. ϕ is the angle between F- and x-axis. Assuming an even magnetic field, the electro-magnetic forces induced by other three wires are identical and can also then be denoted by F. Then the net moment acting on the bobbin is

$$M = 4FD,$$

where D, as shown in Fig. 4b, is the distance between the bobbin center and the wire. The angular deflection θ is next derived for calculating the equivalent rotational (tilting) stiffness k_θ, which is started with expressing the translational deflections in x and y directions due to the total electro-magnetic force F as

$$\delta_x = \frac{4F\cos\phi}{k_x} = \frac{F\cos\phi L^3}{12EI_w} \quad \text{and}$$
$$\delta_y = \frac{4F\sin\phi}{k_y} = \frac{F\sin\phi L^3}{12EI_w} \quad (7)$$

The net deflection along F is

$$\delta = \sqrt{\delta_x^2 + \delta_y^2}. \quad (8)$$

Assuming small motions of the bobbin, thus, $\delta = D\theta$. Henceforth,

$$k_\theta = \frac{M}{\theta} = \frac{4FD}{\delta/D} = \frac{48EI_w\left(D_x^2 + D_y^2\right)}{L^3\sqrt{(D_x/D)^2+(D_x/D)^2}}, \tag{9}$$

where D_x and D_y are, respectively, as shown in Fig. 4b, the distances in x and y directions between the bobbin center and each wire.

2.2 System identification

The prerequisite condition for designing a favorable FLC controller is to build a precise system dynamic model. This precise model is used for evaluating FLC performance before it is tested in the hardware system. The model can be derived by theoretical dynamic characteristics as stated in the previous section or through system identification in this section. The usage of the curve fitting method to identify system dynamic model is used herein for a single degree of freedom system. In general, this modeling method of single degree of freedom system could not satisfy the controller design of multi-axial system which has the coupling between different DOFs. Nevertheless, the intelligent servo controller—FLC, which will be proposed in next section, has capability to overcome the nonlinear coupling among three axes of the optical pickup, although the FLC is designed only based on three independent system dynamic models.

To identify the three independent models, a dynamic signal analyzer is used to obtain the frequency responses of the four-wire type optical pickup as subjected to a swept sine excitations in three different directions. The transfer functions of the real system can then be estimated. Figure 5 shows the whole experiment system for identification, including the dynamic signal analyzer, three-axis optical pickup, power amplifier and displacement sensor. The dynamic signal analyzer provides the input voltage signal, which is powered by an amplifier into the three-axis optical pickup. The optical fiber displacement sensor measures the displacement of the objective lens tip and feedbacks the signal to the signal analyzer. The frequency of the sine wave swept ranges from 5 Hz to 10 kHz. The frequency responses of the real system can be obtained. Figure 6 shows the frequency responses long three directions. The forms of system transfer function to be identified is considered as

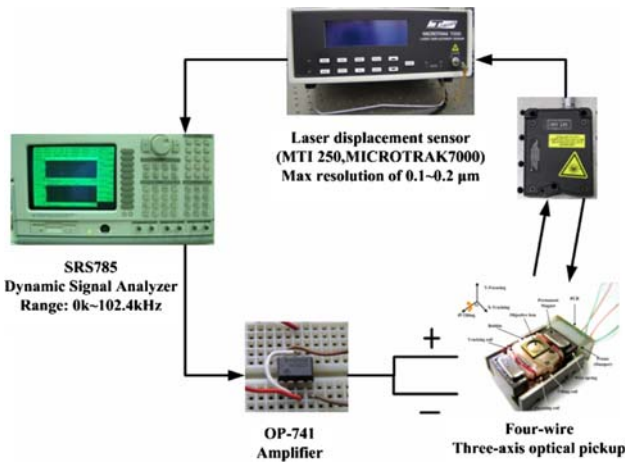

Fig. 5 Experiment system for identification

$$G(s) = \frac{k\omega_n^2}{s^2 + 2\zeta\omega_n s + \omega_n^2}. \tag{10}$$

where ω_n and ζ are the nature frequency and damping ratio, respectively. The damping ratio ζ can be calculated by the following equation

$$|G(j\omega)|_{\max} = \frac{1}{2\zeta\sqrt{1-\zeta^2}}. \tag{11}$$

The gain k in Eq. 10 is computed by the DC gain of the real system by the following equation

$$\text{DC gain} = 20\log\left|\frac{k\omega_n^2}{s^2 + 2\zeta\omega_n + \omega_n^2}\right|_{s=j\omega,\omega=5}. \tag{12}$$

Following the above basic identification procedure in Eqs. 11, and 12, the system transfer function could be identified, yielding

$$G_F(s) = \frac{2.737 \times 10^6}{s^2 + 53.48s + 1.117 \times 10^5}(\mu m/V), \tag{13a}$$

$$G_{Tr}(s) = \frac{3.583 \times 10^6}{s^2 + 55.29s + 1.194 \times 10^5}(\mu m/V), \tag{13b}$$

$$G_{Ti}(s) = \frac{3.5631 \times 10^6}{s^2 + 77.91s + 9.485 \times 10^5}(\mu m/V), \tag{13c}$$

along focusing, tracking and tilting, respectively. The identified system frequency responses are shown in Fig. 6, where it is seen that the responses of the real system and the identified two-order transfer function of system are closely matched before 10 k (rad/s), which is normally beyond the actuation bandwidth of a optical pickup. However, beyond 10 k (rad/s) the responses are different between the real system and the identified model. This is due to noticeable noises from sensors in high frequency.

3 Auto-tuning scheme

The auto-tuning servo scheme is presented in this section. This intelligent control servo is designed based on a commercially often-used double-lead compensator, which

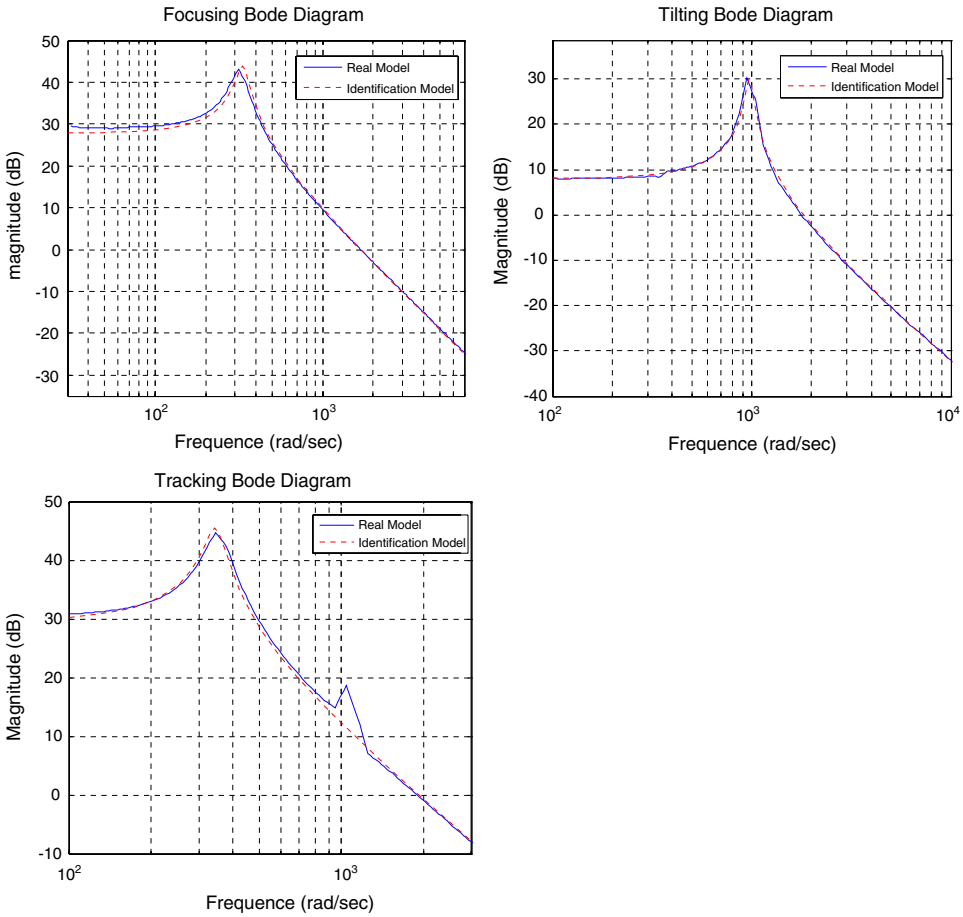

Fig. 6 Frequency responses of real and identified models

is equipped with a fuzzy logic controller for real-time auto-tuning on control parameters. Finally, a genetic algorithm (GA) is used to optimize the auto-tuning process for better performance of pickup positioning.

3.1 Double-lead compensator

For an unstable system, a well-designed phase-lead compensator is employed to increase the phase margin of system for reaching desired stability. Since the desired compensated phase angle is more than 60°, the double-lead compensator is employed to provide enough phase margins for conducting better performance. The system block diagram is shown in Fig. 7, which r is the reference signal; $G_{c1}(s)$ is the first-lead compensator; $G_{c2}(s)$ is the second-lead compensator; K is the loop gain; $1/s$ is an integrator; y is the output signal. Note that in order to eliminate the steady-state error, the system with the double-lead compensator needs to be combined with an integrator. The transfer function of the double-lead compensator is

$$G_c(s) = K\frac{1+a_1T_1s}{1+T_1s}\frac{1+a_2T_2s}{1+T_2s}. \tag{14}$$

where $K > 0$, T_1 & $T_2 > 0$, a_1 & $a_2 > 1$. For simplicity, among parameters K, T_1, T_2, a_1, a_2 of the phase-lead

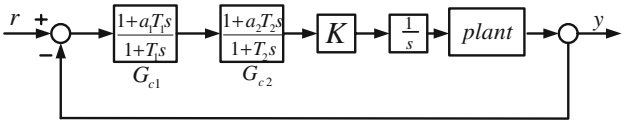

Fig. 7 Block diagram of the double-lead controlled system

compensators, only the parameter a_1 of the first-lead compensator is chosen in this study to be tunable. The design steps of the double-lead compensator in Eq. 14 are stated as below,

1. In order to annihilate the steady-state error, free integrators are added into individual transfer functions in Eqs. 13 for the dynamics along three axes of the pickup, resulting in

$$G_F(s) = \frac{2.737\times10^6}{s(s^2+53.48s+1.117\times10^5)}, \tag{15a}$$

$$G_{Tr}(s) = \frac{3.583\times10^6}{s(s^2+55.29s+1.194\times10^5)}, \tag{15b}$$

$$G_{Ti}(s) = \frac{3.5631\times10^6}{s(s^2+77.91s+9.485\times10^5)}. \tag{15c}$$

2. The frequency responses of the uncompensated open-loop system are shown in Fig. 8. The designed double-lead compensator must satisfy the time domain specifications which are

$$M_p = 0.35(\leq 35\%), T_s = 0.1(\text{sec}), 40^\circ < PM < 60^\circ \tag{16}$$

where M_p is the maximum overshoot; T_s is the settling time and PM is the phase margin. Following a standard procedure, for the systems in Eqs. 15, M_p, T_s and PM can be derived by

$$\text{PM} = \tan^{-1}\left\{2\zeta\left(\frac{1}{\sqrt{4\zeta^4+1-2\zeta^2}}\right)^{\frac{1}{2}}\right\}, \tag{17}$$

$$\begin{cases} M_p = e^{-\pi\zeta 1\sqrt{1-\zeta^2}} \\ T_s = \dfrac{4}{\zeta\omega_n} \end{cases}, \tag{18}$$

$$\omega_b = \omega_n\sqrt{1-2\zeta^2+\sqrt{2-4\zeta^2+4\zeta^4}}, \tag{19}$$

$$\left|K\frac{k\omega_n^2}{s^2+2\zeta\omega_n s+\omega_n^2}\right|_{s=\frac{\omega_b}{2}} = 1, \tag{20}$$

where ζ is the equivalent damping ratio of the systems in Eqs. 15. The desired phase margins are chosen as 57°, 57° and 45° herein for satisfying performance specifications for tracking, focusing and tilting. The damping ratio ζ, the maximum overshoot M_p and the natural frequency ω_n can be computed by Eqs. 17 and 18. The bandwidth of the system ω_b can be solved by substituting ζ and ω_n into Eq. 19 and the loop gain K is derived by Eq. 20.

3. The loop gain K is next multiplied by the transfer function $G(s)$ to produce a new transfer function $G_u(s)$ which is called "uncompensated system". The transfer functions of the uncompensated system are

$$Gu_F(s) = \frac{1.513\times 10^8}{s(s2+53.48s+1.117\times 10^5)}, \tag{21a}$$

$$Gu_{Tr}(s) = \frac{1.196\times 10^8}{s(s^2+55.29s+1.194\times 10^5)}, \tag{21b}$$

$$Gu_{Ti}(s) = \frac{3.5631\times 10^8}{s(s^2+77.91s+9.485\times 10^5)}. \tag{21c}$$

The resulted phase margins of the dynamics along focusing, tracking and tilting are −81.9°, −81.3° and −74.1°, respectively, while the gain margins are −26.4, −25.2 and −13.7 dB, respectively. The gain-crossover frequencies ω_g are 572, 572 and 1,120 rad/s as shown in Fig. 7. According to the above computation results, the differences between the phase margin of $G_u(s)$'s in Eqs. 21 and the desired phase margin is more than 90°, thus failing to stabilize the systems. To solve the problem, in the next step, the first-lead compensator is designed to improve the phase margin of the uncompensated systems.

4. Having added the first phase-lead compensator into the system, the phase margin of system could be improved to about −10°. With the first phase-lead compensator in hand, a newly computed gain-crossover frequency ω_{g1}^* of system which is larger than the original one, thus improving the phase margin. Note that the phase margin drops moderately as compared to theoretical expected value by the aforementioned computation process, since ω_{g1}^* is not located at the maximum phase. In order to achieve the desired phase margin, the estimated value ε_1 for the difference between the final desired phase margin and the originally uncompensated margin is necessarily computed. The correlative equation is then

$$\phi_{m1} = \phi_{d1} - \phi_1 + \varepsilon_1, \tag{22}$$

where ϕ_{d1} is the desired phase margin, ϕ_1 is the phase margin of the uncompensated system, ϕ_{m1} is the phase angle which is needed to be compensated. The compensation ϕ_{m1} is accomplished by assigning a_1 in Eq. 14 by

$$a_1 = \frac{1+\sin\phi_{m1}}{1-\sin\phi_{m1}}. \tag{23}$$

Substituting the desired ϕ_{m1} 's into Eq. 23, the parameter a_1 of the first phase-lead controller can be derived. The derived a_1's for each of three axes are 91.79, 101.51 and 787.8, respectively.

5. Define ω_{m1} as the frequency of the maximum phase margin. When $\omega_{m1} = \omega_{g1,}^*$, the first phase-lead compensator will provide 10 log a_1 dB for the gain at the maximum phase margin. Thus ω_{g1}^* can be computed by

$$20\log\left|G_u\left(j\omega_{g1}^*\right)\right| = -10\log a_1. \tag{24}$$

The parameter T_1 of the first phase-lead compensator in Eq. 14 can be derived by substituting a_1 and ω_{m1} into

$$T_1 = \frac{1}{\omega_{g1}^*\sqrt{a_1}}. \tag{25}$$

Finally, the transfer function of the first phase-lead compensator is

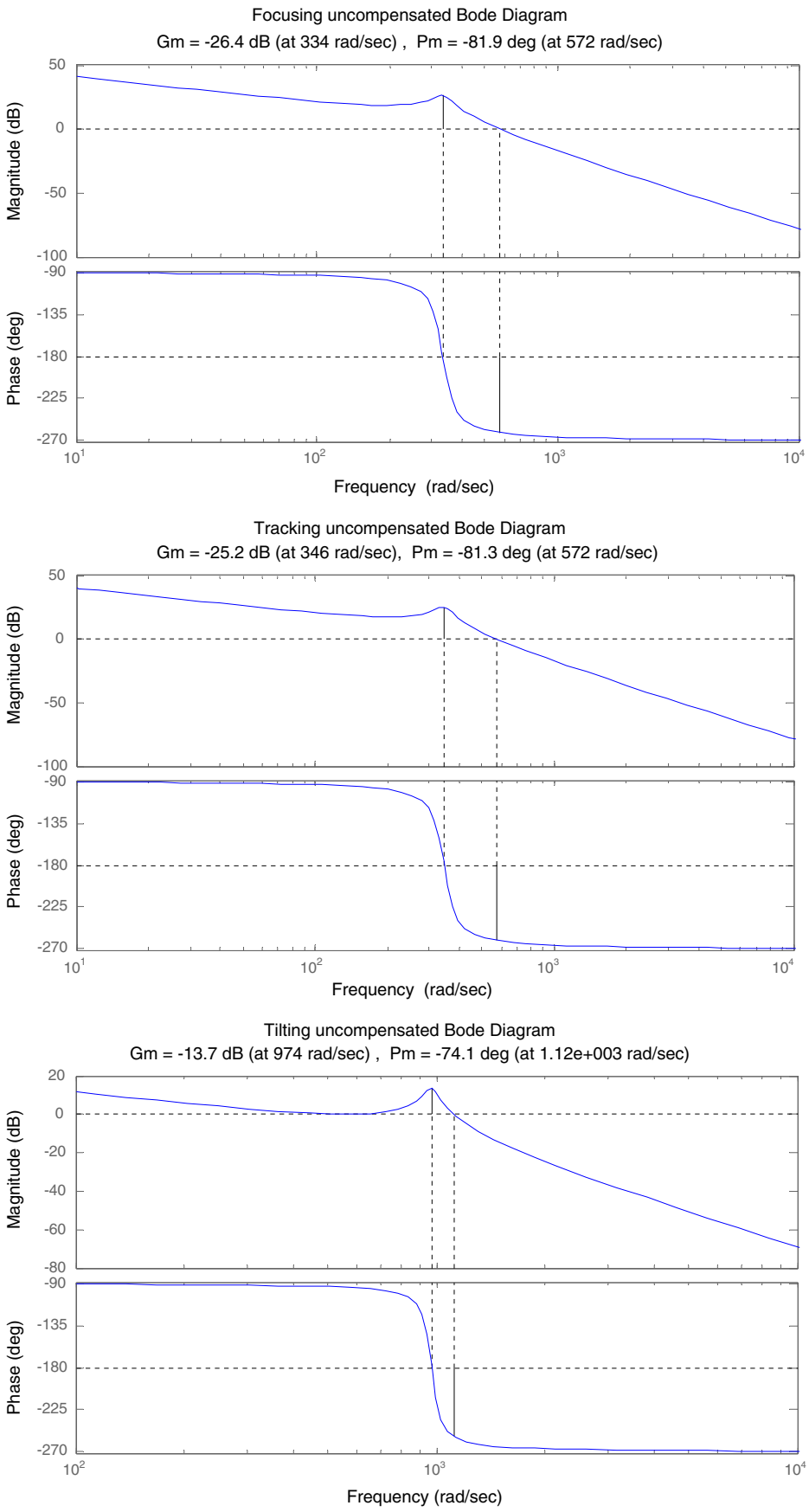

Fig. 8 Uncompensated systems

$$Gc_1(s) = \frac{1 + a_1 T_1 s}{1 + T_1 s} \tag{26}$$

The phase margins and gain margins of the compensated systems along focusing, tracking and tilting with the help from the first phase-lead compensator in Eq. 26 are $-8.83°$ and -23.1 dB, $-8.15°$ and -21.7 dB, $-1.72°$ and -8.34 dB, respectively. The frequency response is depicted in Fig. 9.

6. The design process of the second phase-lead compensator is the same as the first one. The transfer function of the second phase-lead compensator is

$$Gc_2(s) = \frac{1 + a_2 T_2 s}{1 + T_2 s}. \tag{27}$$

The transfer functions of the double-lead compensator are finally derived as

$$Gc_F(s) = 55.3 \times \frac{1 + 0.008754s}{1 + 0.00009537s} \times \frac{1 + 0.002413s}{1 + 0.0006167s} \tag{28a}$$

$$Gc_{Tr}(s) = 33.48 \times \frac{1 + 0.009142s}{1 + 0.00009006s} \times \frac{1 + 0.002352s}{1 + 0.0006478s} \tag{28b}$$

$$Gc_{Ti}(s) = 100.0 \times \frac{1 + 0.0122s}{1 + 0.00001549s} \times \frac{1 + 0.0007517s}{1 + 0.0001067s} \tag{28c}$$

Figure 10 shows the phase margins and gain margins are 56.6° and 19.5 dB, 57 and 19.6 dB, 45.6° and 25.5 dB, respectively, for focusing, tracking and tilting, which satisfy the original time-domain specifications as listed in Table 1.

3.2 Auto-tuning algorithm

Some parameters of the designed controllers are tuned in off-line fashion. The process consumes time and cost. The method developed herein tunes the parameters automatically in an on-line fashion to expedite the development of the pickup servo. First, the double-lead compensator is chosen to be the base controller which is designed in previous sections. Second, the fuzzy logic controller is used to tune the parameter a_1 of the double-lead compensator to perform dynamic decoupling and forge the control efforts toward the goals of precision positioning. Finally, a genetic algorithm is employed off-line to search the optimal membership functions of the fuzzy logic controller (FLC) to render better performance.

3.2.1 *Fuzzy logic controller*

The structure of the double-lead compensator with FLC is called fuzzy double-lead controller. The structure is illustrated in Fig. 11. Previous sections accomplish design of the double-lead compensator. The fuzzy logic controller is synthesized herein to tune the parameters of the double-lead compensator, the process of which consists of (1) defining inputs and outputs of FLC; (2) fuzzification; (3) rule table; (4) defuzzification.

3.2.1.1 Defining inputs and outputs of FLC The control output error $e(t)$ and the increment of terror $de(t)$ are chosen to be considered as the input signals to FLC. Therefore,

$$e(t) = r(t) - y(t), \tag{29}$$

$$de(t) = e(t+1) - e(t) \tag{30}$$

where $r(t)$ is the reference signal and $y(t)$ is the output signal of the system. The FLC is intended to tune the performance of a standard phase-lead compensator

$$C(s) = \frac{1 + aTs}{1 + Ts} \qquad T > 0, \quad a > 1. \tag{31}$$

where a and T can be designated to move the zero and pole of the $C(s)$ in the s-plane, as shown in Fig. 12. Two different kinds of movements for zeros and poles can be realized. They are

1) Moving $-1/aT$ to the origin will improve the rising and settling times; however, the maximum overshoot will be increased with $-1/aT$ closing the origin.
2) Moving $-1/T$ far away the origin will decrease the maximum overshoot; however, the rising and settling times will be increase as T becomes small.

According to above two points, the performance of the system can be decided by tuning a and T. In order to simplify the auto-tuning system and increase the effectiveness of computation, only one parameter a of a phase-lead compensator is tuned. The parameter a_1 of the first-lead compensator in Eq. 14 is chosen herein.

3.2.1.2 Fuzzification Fuzzification is the process of decomposing system input, output signals into one or more fuzzy sets. In order to fuzzify input/output signals, the membership functions are first defined. Many types of membership functions can be used, but the triangular or trapezoidal shaped ones are the most common because they are easier to be computed during fuzzification and later defuzzification. Figure 13 shows triangular membership functions used in this study for inputs and outputs of the system. The inputs are error and error increments defined in Eqs. 29 and 30, while the output is the value of a_1 previously given in Eq. 14. Note that normalizations are applied to the error and error increment before fuzzification. The scaling factors for normalizations are chosen such that the error and

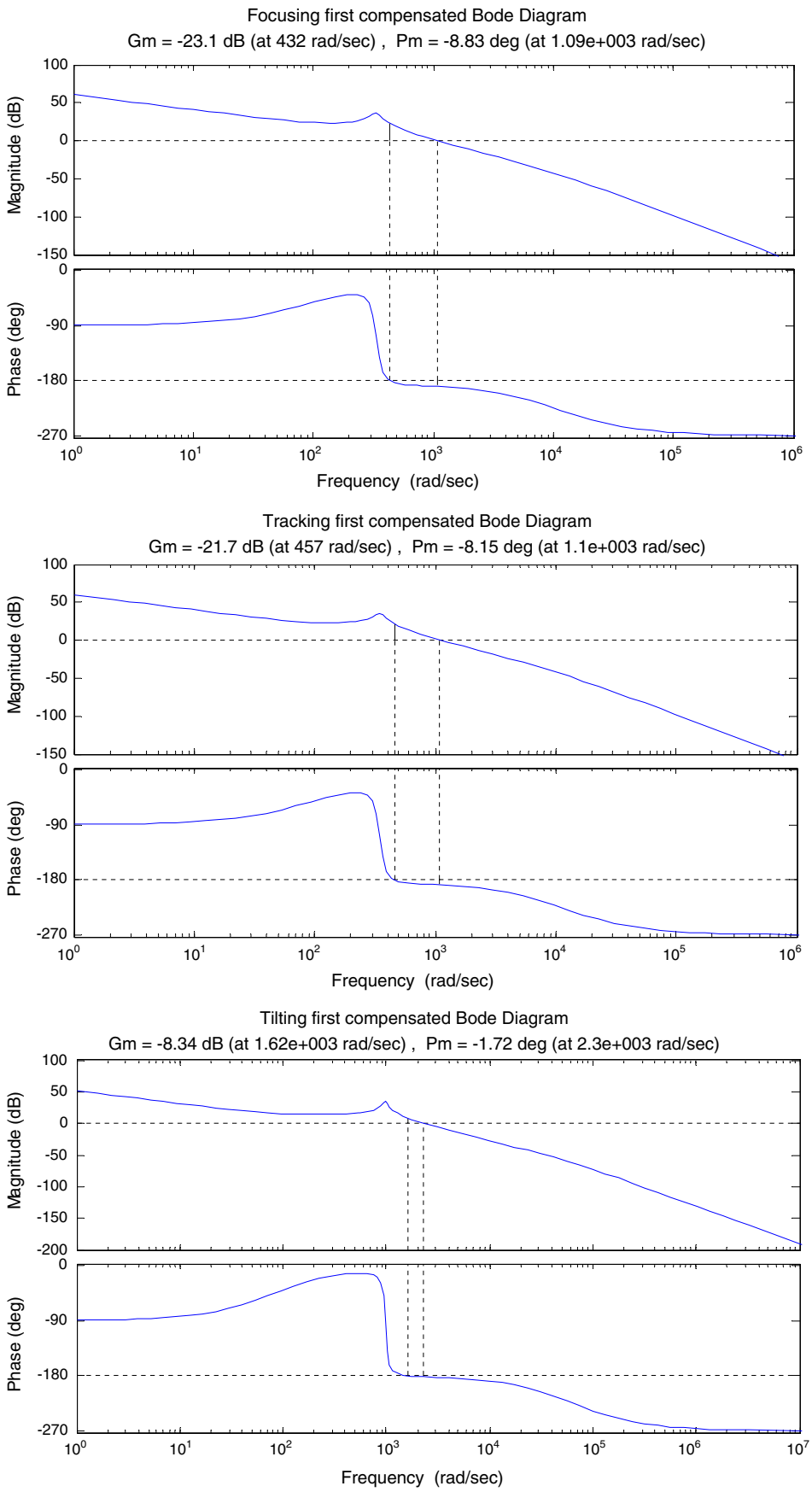

Fig. 9 The systems compensated by the first-lead compensator

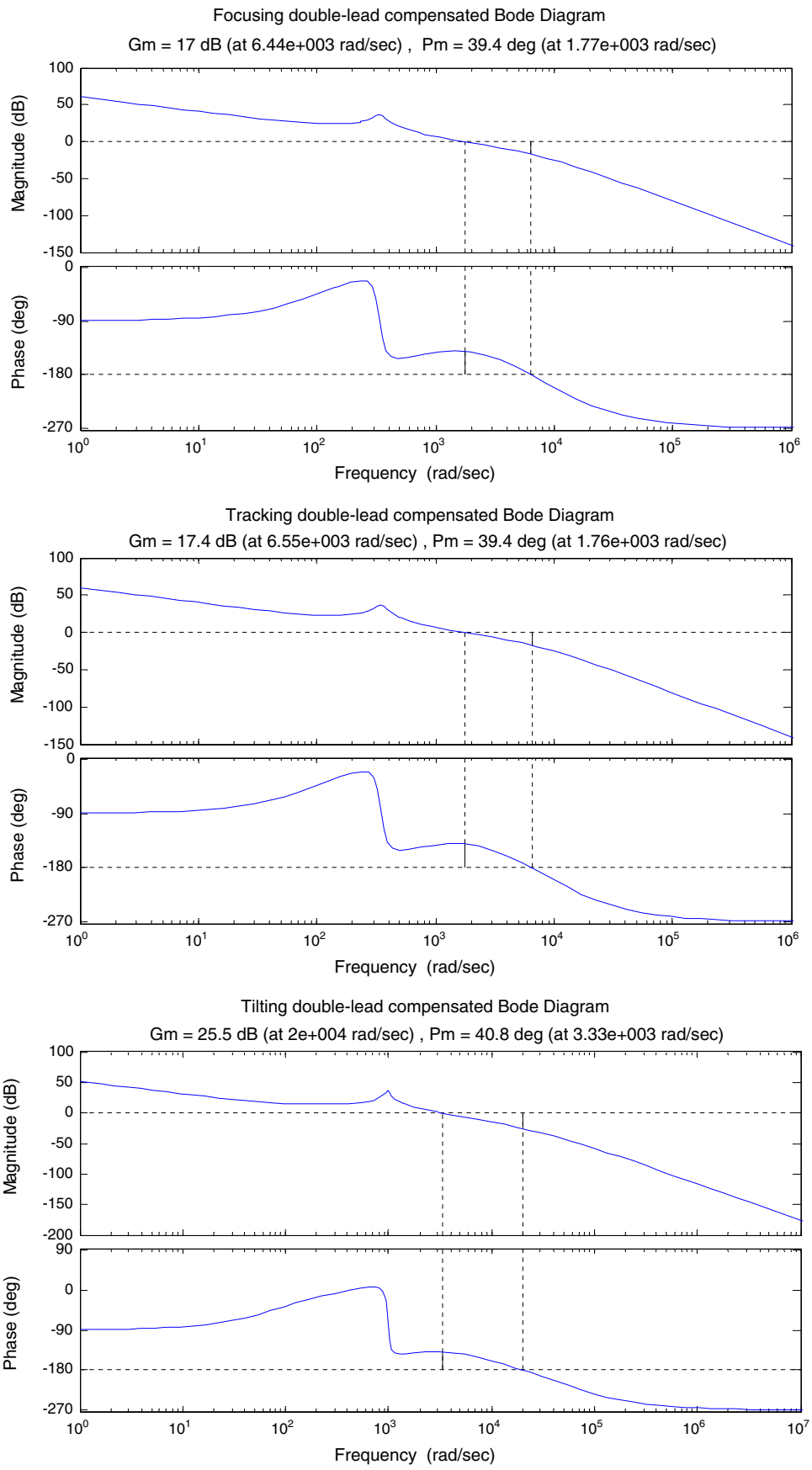

Fig. 10 The systems with the double-lead compensator

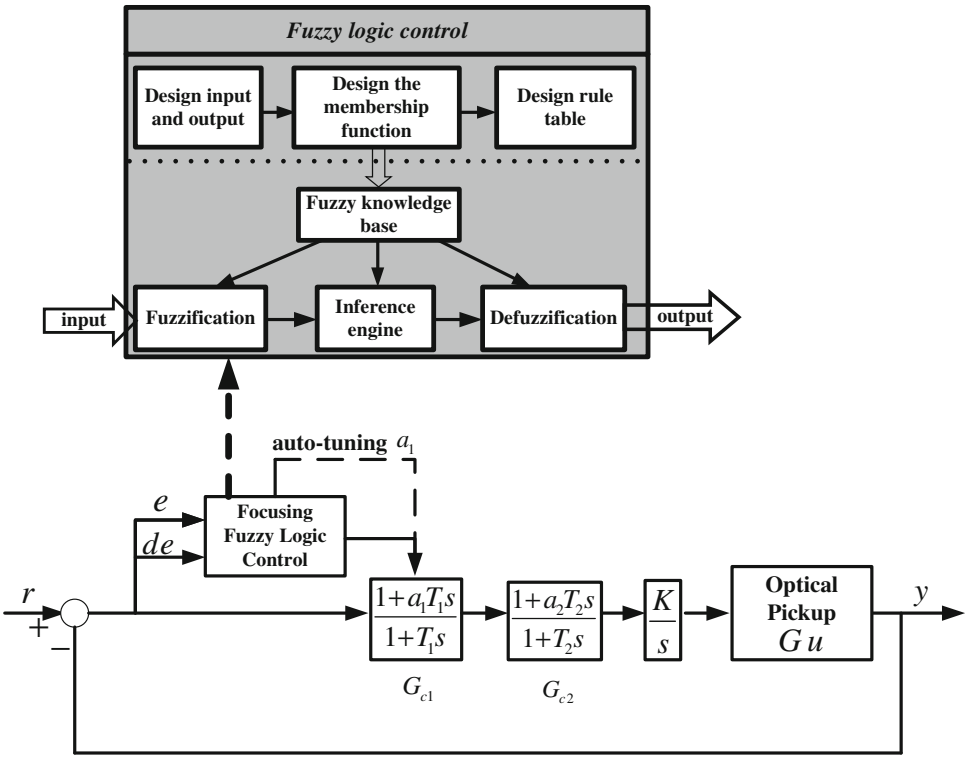

Fig. 11 The structure of the fuzzy double-lead controller

error increment are large enough to span the interval [−1, 1]. Note in Fig. 13 that the membership functions overlap to allow smooth mapping of fuzzification. The process of fuzzification allows the system inputs and outputs to be expressed in linguistic terms such that the control rules can be applied in a simple manner. The membership functions for parameter a_1 in the first phase-lead compensator in Eq. 14 are determined such that different values of a_1 are expected to achieve desired control goals.

3.2.1.3 Rule table Having completed fuzzification, efforts are paid next to establish linguistic rules regulating the input/output relations. This starts with understanding on the typical step responses for the focusing and tracking in Fig. 14a and that for tilting in Fig. 14b, where it is seen that initial positions of the pickup along focusing and tracking direction are defined as negative and then to a zero value at steady state, while the initial tilting angle is zero since the pickup is initially in horizontal equilibrium. There are also corresponding histories of positioning error $e(t)$ and increment of error $de(t)$ depicted in Fig. 14. As depicted in Fig. 14, different time instants a − h are chosen for forging the aforementioned linguistic rules that regulates the relation from the inputs, $e(t)$ and $de(t)$ to the output, the parameter a_1 in the first-lead compensator in Eq. 14. The forged linguistic rules are listed in the two rule tables in Fig. 15 for focusing and tilting, respectively.

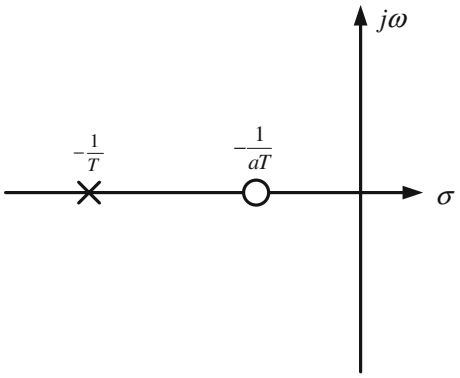

Fig. 12 S-plane of the phase-lead compensator

At varied time instants a−h denoted in Fig. 14a, there are different combinations of magnitudes and signs of $e(t)$ and $de(t)$. The considered combinations are NB, NS, NM, ZE, PS, PM, PB, where S stands for Small, M for Medium, B for Big and ZE for Zero, while N for negative and P for positive. It is seen from Fig. 15a, b that a quasi-orbit is formed instants a to h, which correspond to zero $e(t)$ and $de(t)$, meaning that the control goal is achieved. For each combination in every square in both tables, a linguistic rule relating from $e(t)$ and $de(t)$ to a_1 needs to be proposed. The rule is proposed based on the general effects of $e(t)$ and $de(t)$ that (1) when $e(t)$ is large, a_1 should be tuned to decrease the maximum overshoot, following design guideline 2 in Sect. 3.2.1.1 for movement of zero and pole

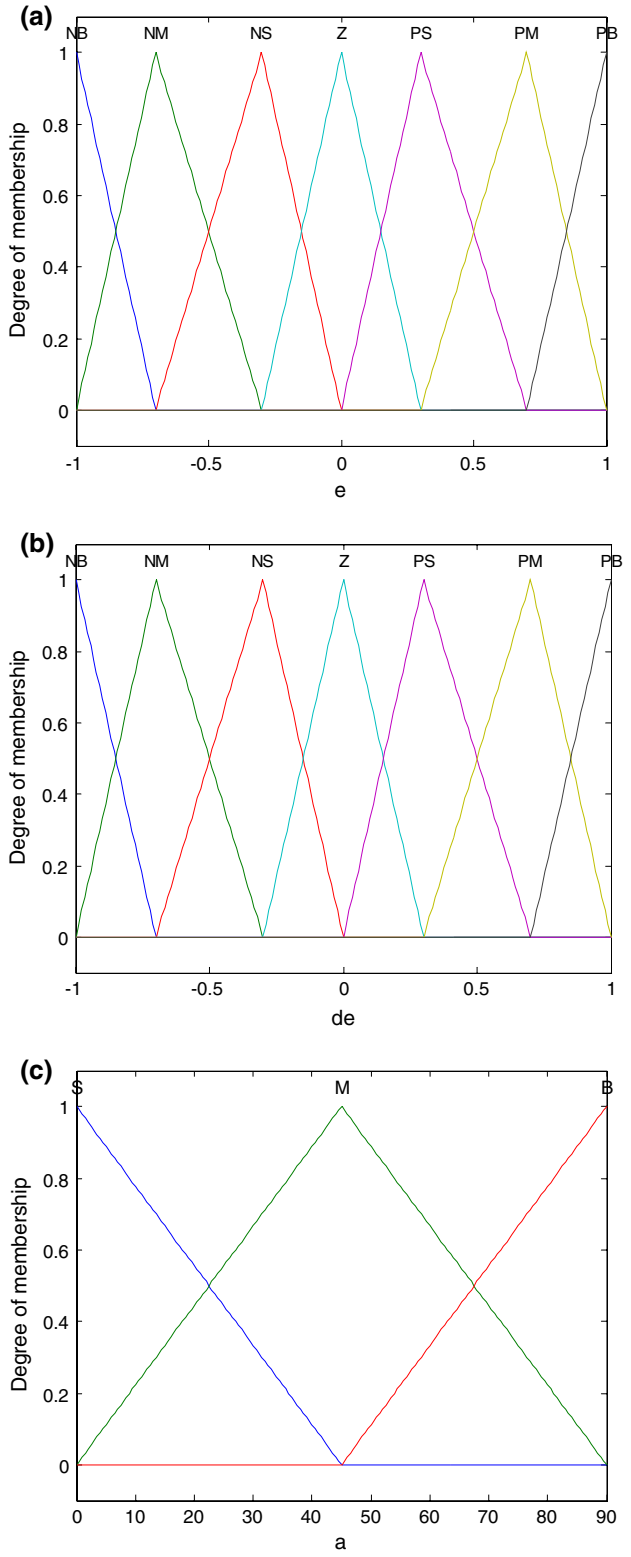

Fig. 13 Triangular membership functions

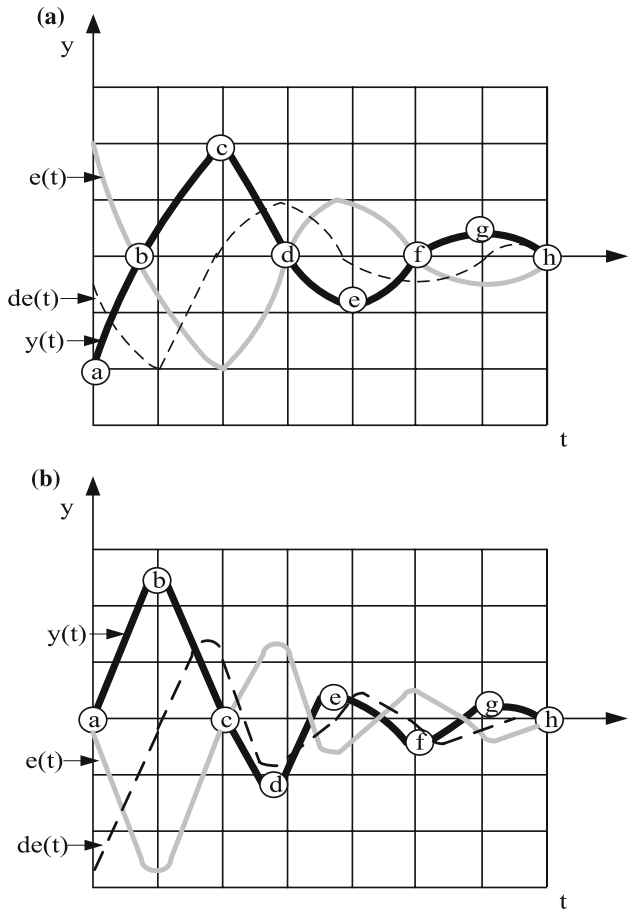

Fig. 14 Typical step response for **a** focusing and tracking directions; **b** tilting direction

of the first-lead compensator in Eq. 14; (2) when $de(t)$ is large, a_1 should be tuned to decrease rising and settling times, following design guideline 1 in Sect. 3.2.1.1. Based on the above general guidelines, 49 rules can be forged. They are listed in Table 2. For example, near to the instant b in Fig. 15a, the error $e(t)$ is close to zero while the increment of the error $de(t)$ is negative and medium. At this point, in order to avoid a large overshoot, a_1 is tuned to a small value, following guideline 2; thus, rule 23 is

> if "$e(t)$ is **ZE**" and "$de(t)$ is **NB**" then "a is **SMALL**".

3.2.1.4 Defuzzification Having forged fuzzy reasoning, linguistic output variables from applying Table 2 need to be converted into numerical valued. The intension herein is to derive a single exact numeric value that best represents the inferred fuzzy values of the linguistic output variable. Defuzzification is such inverse transformation which maps the output from the fuzzy domain back into the numerical domain. The Center-of-Area (COA) method is chosen herein to complete the job, which is often referred to as the Center-of-Gravity (COG) method because it computes the centroid of the composite area representing the output fuzzy variables.

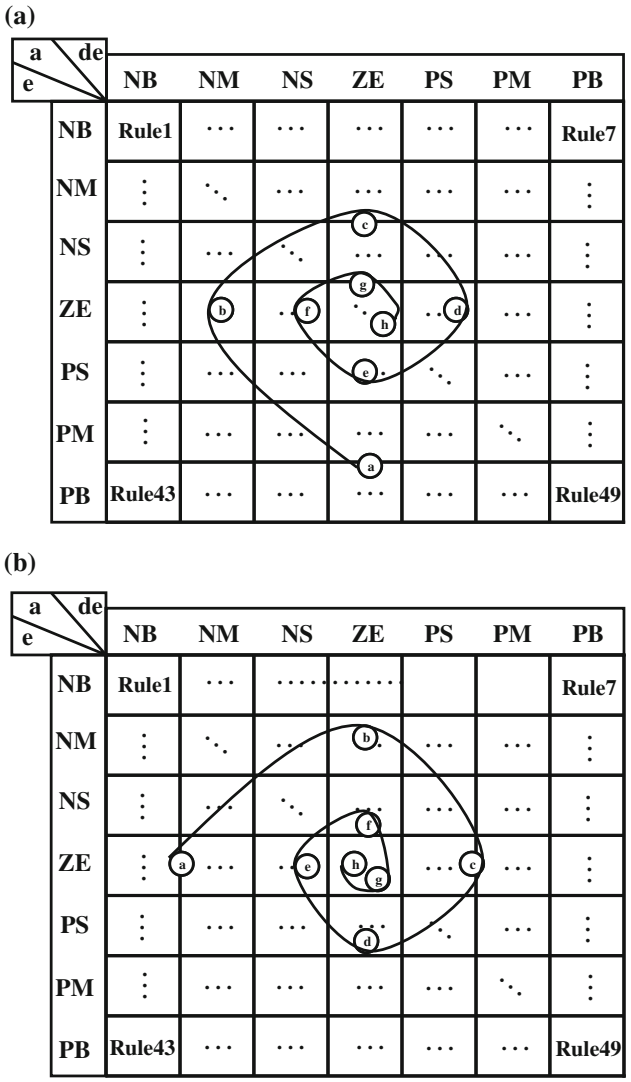

Fig. 15 Loci of time instants in Fig. 14 for **a** focusing and tracking; **b** tilting directions

3.2.2 *Genetic algorithm*

The main difficulty in FLC design and are the choices of proper membership functions and the associated adaptive gains. This subsection develops the application of a genetic algorithm (GA) technique in selecting the membership functions and the adaptive gain. A flow chart of a genetic algorithm is shown in Fig. 16. First, choose the number of parameters need to be searched by GA. Then define the initial population. These parameters are coded to binary type and the fitness value is the defined and computed by GA to find the best parameters. Selection from the first generation of better parameters is reserved to next generation and compared with other parameters to search much better parameters in the second generation. Finally, the best parameters are derived and the maximum fitness value is reached.

Table 2 Rule table

e(t)	*de*(*t*)						
	NB	NM	NS	ZE	PS	PM	PB
Focusing rule table							
NB	B	B	B	B	B	B	B
NM	M	M	M	B	M	S	S
NS	S	S	M	M	S	S	S
ZE	S	S	S	M	S	S	S
PS	S	S	S	M	M	S	S
PM	S	S	M	B	M	M	M
PB	B	B	B	B	B	B	B
Tracking rule table							
NB	B	B	B	B	B	B	B
NM	M	M	M	B	M	S	S
NS	S	S	M	M	S	S	S
ZE	S	S	S	M	S	S	S
PS	S	S	S	M	M	S	S
PM	S	S	M	B	M	M	M
PB	B	B	B	B	B	B	B
Tilting rule table							
NB	M	M	B	M	S	S	S
NM	S	M	M	S	S	S	S
NS	S	S	M	S	S	S	S
ZE	S	S	M	M	S	S	S
PS	S	M	B	M	M	M	M
PM	B	B	B	B	B	B	M
PB	B	B	B	B	B	B	B

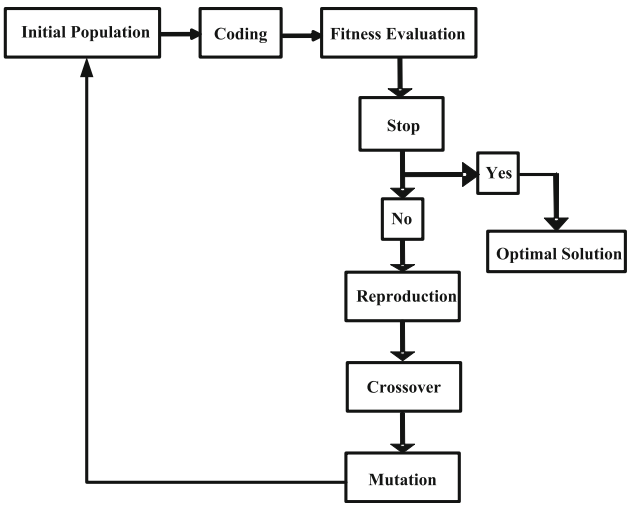

Fig. 16 A flow chart of a genetic algorithm

3.2.2.1 Genetic algorithm for fuzzy double-lead controller A membership function in general has three important parameters to be specified: shape, distance and peak location, as described in Fig. 17. Among those three values, the peak value of the triangle plays a key role in improving or

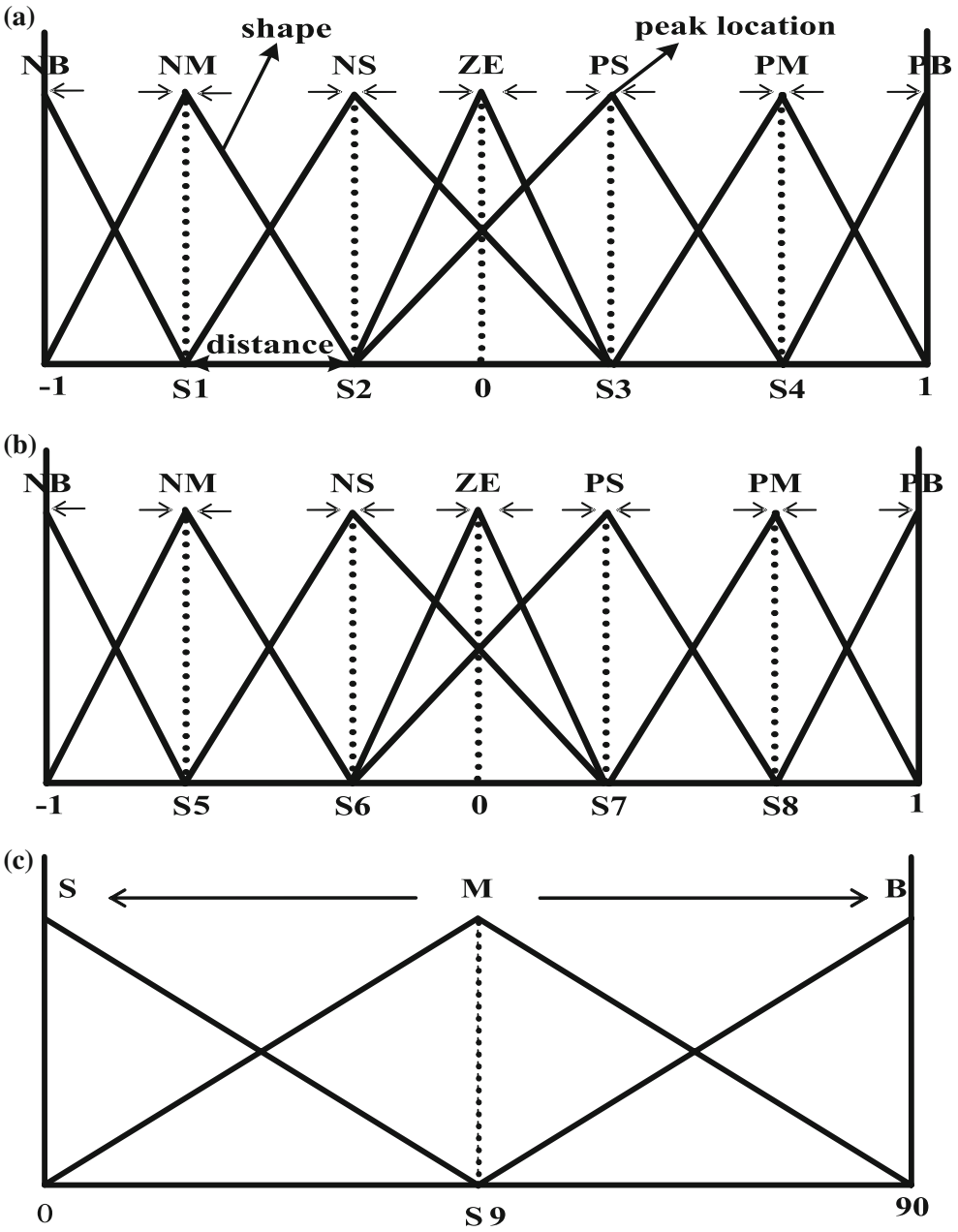

Fig. 17 Membership functions for **a** the error; **b** the increment of error. **c** the parameter "*a*"

degrading the performance of the controller. Different peak values generate different shapes of triangular membership functions. The four parameters to be specified in this study are those at points **S1**, **S2**, **S3**, **S4**, in Fig. 17a; at points **S5**, **S6**, **S7**, **S8**, in Fig. 17b, while at point **S19** in Fig. 17c. The scaling factors **Se** and **Sde** are also considered to be the parameters for searching. Therefore, eleven parameters in total are searched by GA. The use of GA provides a stochastic optimization procedure to search for optimal parameter sets such that the controller performance can be improved. A population is initialized by setting up a random distribution of parameter vectors (incorporates the eleven parameters to optimize). The individual parameter values are assumed with a uniform distribution across the allowable ranges.

GA works with a population of binary strings, not the parameters themselves. Before executing its algorithm, it is necessary to consider how a vector of values from the parameter set is converted to a binary string. The choice of coding length of each element in the vector is concerned with not only the resolution assigned by the designer in the corresponding search space, but also the type of spacings, such as logarithmic or linear spacings. In the binary coding method, the bit length 8 with linear spacing is adopted in this study for each element. As a result, the parameters of membership function can be transformed into a binary

Table 3 Parameters of genetic algorithm

Description	Focusing	Tracking	Tilting
Initial population	60	60	60
Generations	100	100	100
Bit length	8	8	8
Reproduction	Roulette wheel selection	Roulette wheel selection	Roulette wheel selection
Crossover rate	0.7	0.7	0.8
Mutation rate	0.05	0.05	0.07
First-lead "a" range	0 ↓ 90	0 ↓ 90	0 ↓ 120

string with the bit length 104, and then the search space is formed. The decoding procedure is a reverse process of coding.

The cost function is chosen as a more general time-domain weighted error criterion and defined as

$$J = \sum_{t=0}^{l} |\bar{e}(t)|, \tag{32}$$

where $e(t) = r(t) - y(t)$. Then the accumulated error is mapped into a fitness value to fit into the genetic algorithm. The fitness value can be regarded as how well a FLC can be tuned based on the string to actually minimize the error. The higher fitness value implies that the corresponding

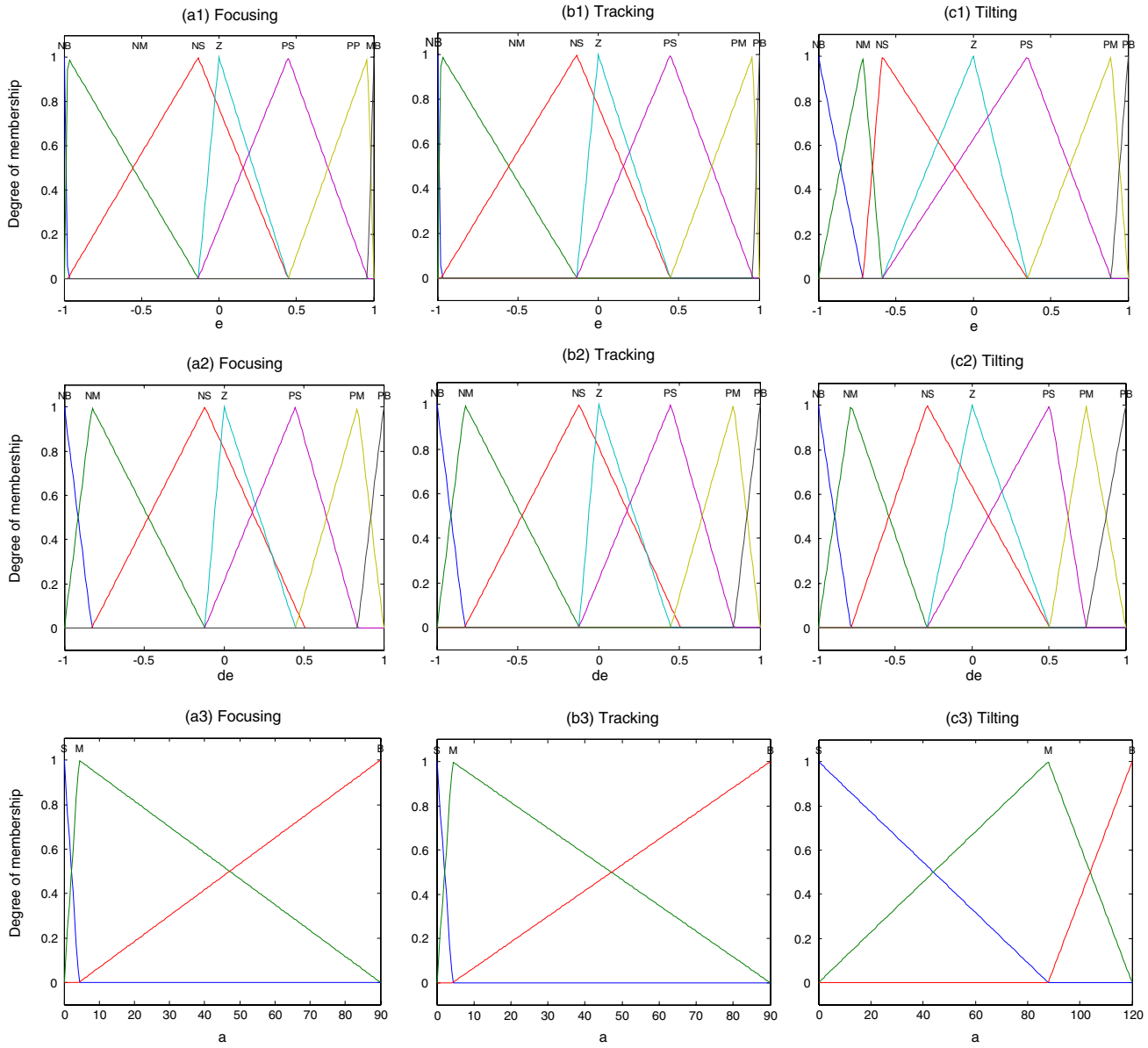

Fig. 18 Definitions of triangular membership functions

string leads to a better solution. GA selects a parent with higher fitness values to generate better offspring. Therefore, a better FLC could be obtained by better fitness in GA. There are several methods to perform the mapping from a cost value to a fitness value. The windowing techniques using linear mapping is considered and the equation is given by

$$\text{Fitness value} = \frac{Q}{J}, \tag{33}$$

where Q must be positive.

These GA operation are performed in a standard manner. Individuals are selected for breeding with a probability proportional to their fitness. For example, in the roulette wheel selection method, the ith string with high fitness value, H_i, is given a proportionately high probability of reproduction, R_i, according to the distribution

$$R_{i.} = \frac{H_i}{\sum H_i}. \tag{34}$$

Once the strings are reproduced or copied for possible use in the next generation, they are put into a mating pool where they await further processing via crossover and mutation. After reproduction, simple crossover proceeds in three steps. First, two newly reproduced individuals from the mating pool are selected. Second, a cross point along the two strings is chosen uniformly at random. Third, the exchange of the characters following the crossover point is performed. Mutation is a rarely used random search operation, which increases the variability of the population in the mating pool and enhances GA performance to find a globally near-optimal solution.

According to above definition, the parameters of GA are listed in Table 3. After the computation by GA, Fig. 18 shows the optimized membership functions which are obviously different from Fig. 13, while Fig. 19 shows the corresponding convergent histories of fitness values for the dynamics in focusing, tracking and tilting. Based on the obtained results in Figs. 18 and 19, the best memberships of the FLC are successfully found by GA.

4 Numerical simulation and experimental validation

Numerical simulations are conducted in this section to confirm the efficiency of the auto-tuning algorithm by checking if performance specifications are satisfies with expected counterparts. The designed auto-tuning algorithm is applied to three-axis optical pickups and the efficiency of this auto-tuning algorithm could be achieved via experimental validation. Figure 20 shows the implementation of the experimental system, which is accomplished mainly

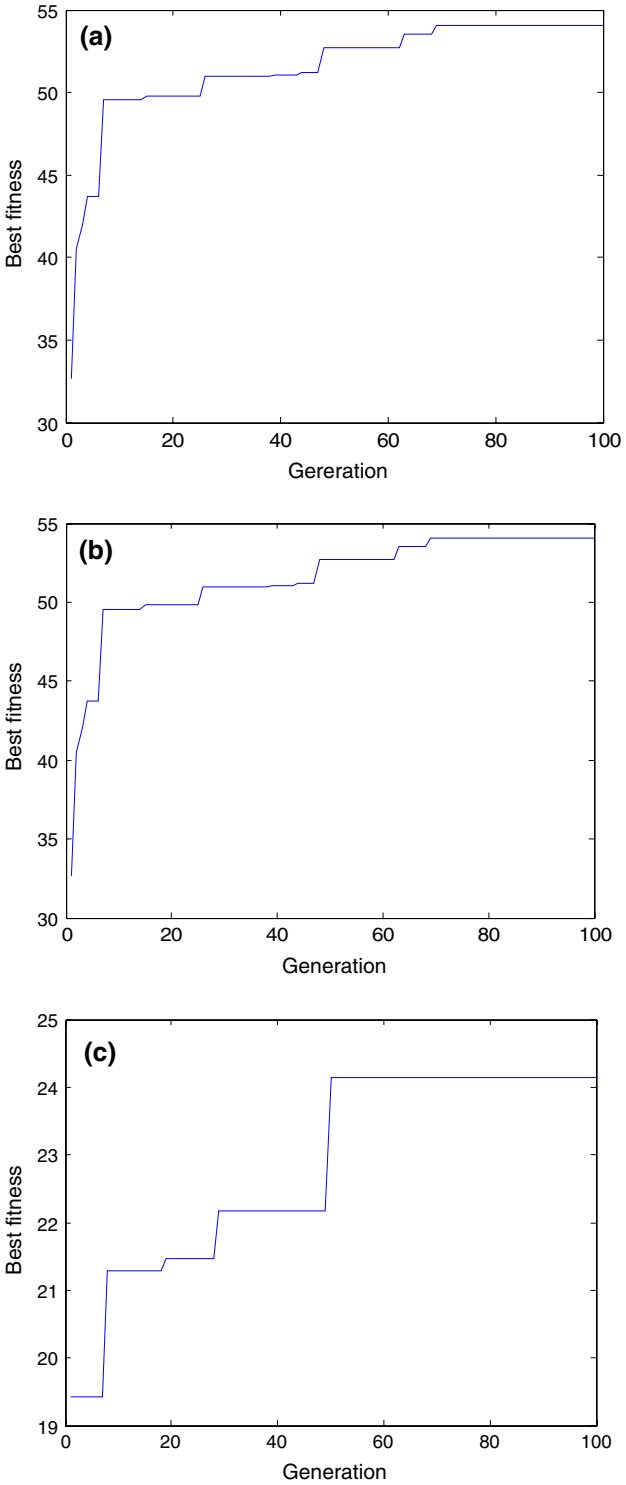

Fig. 19 Fitness value histories of the designed fuzzy double-lead controller in three directions; **a** focusing; **b** tracking; **c** tilting

by the dSPACE module. The output control signals are amplified by an OP-741 amplifier circuit to provide enough and safe input voltage to drive the pickup bobbin. The motions in the three directions of pickup are

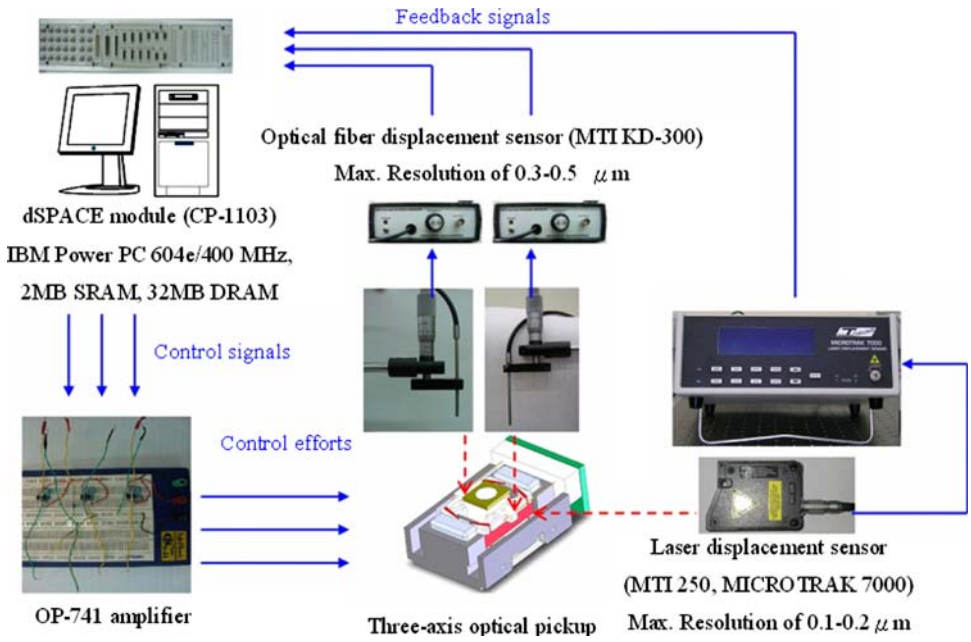

Fig. 20 Experiment system

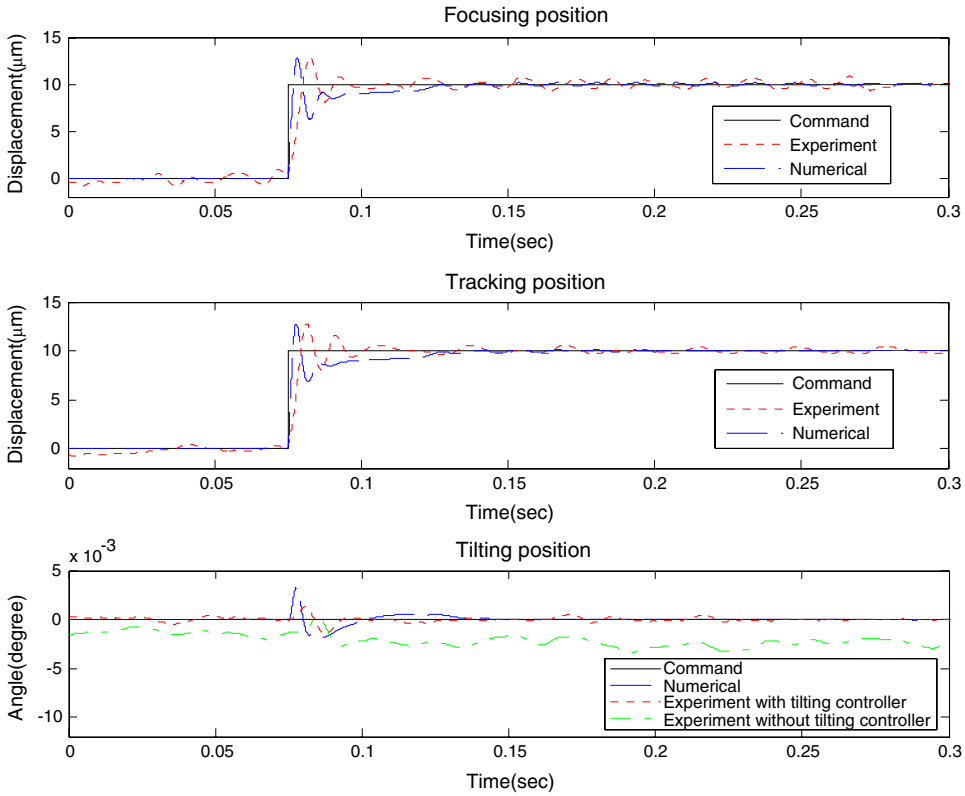

Fig. 21 The actual responses of the three-axis optical pickup using the fuzzy double-lead controller

measured by a laser displacement sensor (MTI 250, MICROTRAK 7000) and two optical fiber displacement sensors, respectively. The sensor signals are feedbacked to dSPACE module that has the compiled auto-tuning algorithm to compute the control effort in real time fashion and then rendering precision positioning of the pickup. Note that the resolution of the laser displacement is ±0.5–0.6 μm and the resolutions of the optical fiber displacement sensors are ±1–2 μm.

4.1 Fuzzy logic double-lead controller

Figure 21 shows the numerical and experimental step responses of the closed-loop system with the fuzzy

Table 4 Time domain specifications of fuzzy double-lead controller

Direction		Maximum overshoot (M_p) (%)	Settling time (T_s) (s)
Focusing	Numerical	27.5	0.059
	Experimental	27.5	0.062
Tracking	Numerical	28	0.06
	Experimental	28	0.062
Tilting	Numerical	32	0.0645
	Experimental	17	0.0645

double-lead controller. In this case, the designed position set as 10 μm in both focusing while in the tracking direction, it is set as zero degree. It can be seen from this figure that the pickup reaches the expected position in three directions during a short settling time period simultaneously. The numerical and experimental performances of the designed fuzzy double-lead controller are characterized in Table 4 by different pre-defined performance indices. Based on these results, the auto-tuning algorithm has the capability to overcome the model uncertainties of the pickups caused by manufacturing tolerance and the couplings among three different DOFs of the three-axis pickup, to reach zero tilting degree in a short period of settling time. This capability can be verified not only in numerical but also experimental data. Also seen from third subfigure of Fig. 21, the experimental responses without a tilting controller activated have much more error than those with a tilting controller. Moreover, it is also seen from Fig. 21 that the experimental responses have slight time delays than the numerical counterparts. This is caused by the application of low-pass filter in experiments, which is intended to reduce the unavoidable sensor noises in experiment. The corresponding errors are shown in Fig. 22, while Fig. 23 shows control efforts.

4.2 Genetic algorithm applied to FLC memberships

In order to attain better performance, the genetic algorithm was designed to seek optimum membership functions of the previously designed fuzzy double-lead controller in priori an off-line fashion. Figure 24 show the responses in three different directions of the controlled pickup. The corresponding time-domain performance of the fuzzy double-lead controller assisted with GA is summarized in Table 5. Comparing Tables 4 and 5, it can concluded that with well

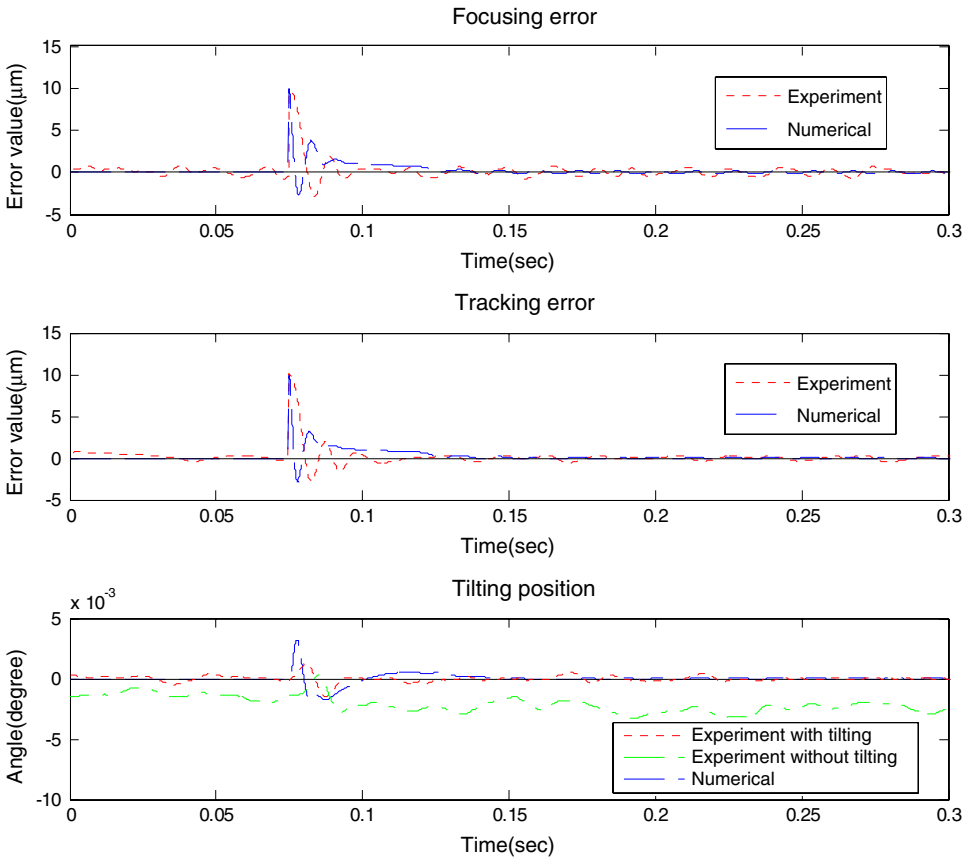

Fig. 22 The position error by the fuzzy double-lead controller of three-axis optical pickup

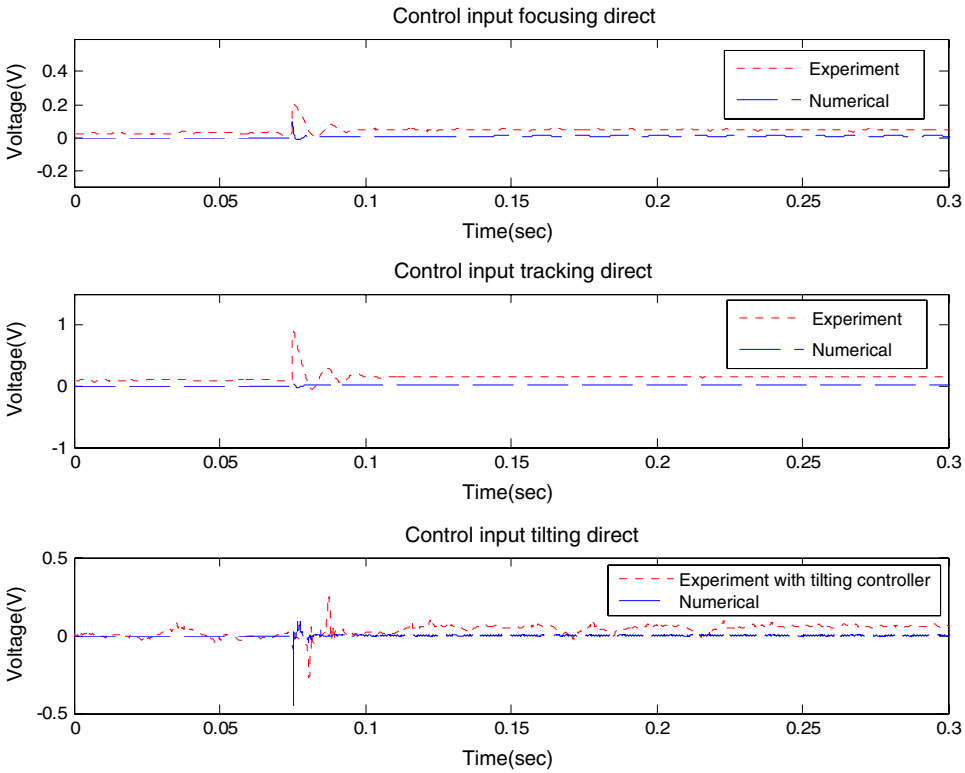

Fig. 23 The control effort by the fuzzy double-lead controller of three-axis optical pickup

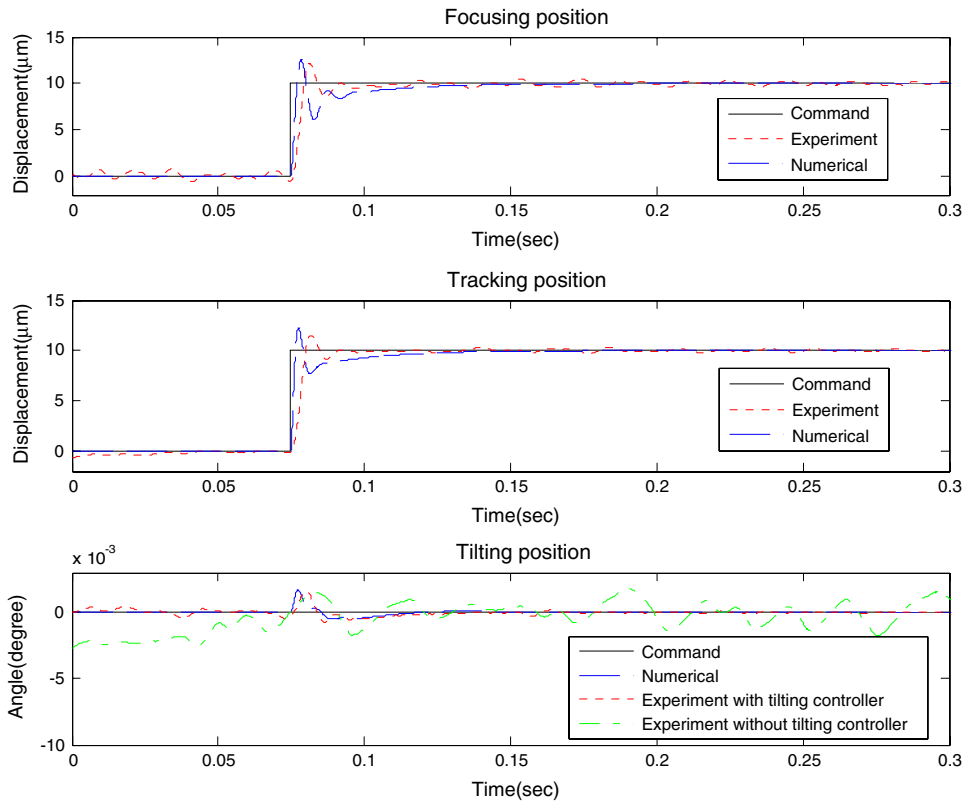

Fig. 24 The actual responses of the three-axis optical pickup using the fuzzy double-lead controller equipped with a genetic algorithm

searched membership functions in hand, the less maximum overshoot and the shorter settling time than the case without genetic algorithm would be guaranteed, as shown in Fig. 24 and Table 5. On the other hand, Fig. 25 shows the corresponding error which is close to zero at steady state, while Fig. 26 shows the required control efforts.

Table 5 Time domain specifications of fuzzy double-lead controller with GA

Direction		Maximum overshoot (M_p) (%)	Settling time (T_s) (s)
Focusing	Numerical	21	0.215
	Experimental	20	0.0315
Tracking	Numerical	20	0.0315
	Experimental	18	0.0315
Tilting	Numerical	17	0.0215
	Experimental	16	0.05

4.3 Error analysis

In order to verify the expected performance of the fuzzy double-lead controller tuned by the genetic algorithm—the capability of overcoming the model uncertainties of the pickups caused by manufacturing tolerance and the couplings among the dynamics in three directions of the pickup, the positioning error analysis concerning two different pickups is conducted herein with first defining the positioning error as

$$E_t = \sqrt{\sum_{i=1}^{n} P_{\exp}^2(i)}, \tag{35}$$

where n is the number of the experimental samples, $P_{\exp}$ is the experimental positioning errors. The total error is defined as below the root mean square value of E_t thus

$$\mathrm{RMSE} = \frac{E_t}{n}. \tag{36}$$

As shown in Figs. 27, 28, 29, although the fuzzy double-lead controller with the assistance from a genetic algorithm was applied for two different pickups, No. 1 and 2, the performances of these two pickups are still similar to each other. On the other hand, the error analysis for these cases, where 8,000 samples are taken from total time-domain responses in each case, results in that the total errors and the root mean square error (RMSE) of the pickup No. 1 are, respectively, 77.34 and 0.0097 μm for the focusing direction, 74.69 and 0.0093 μm for the tracking direction, and 0.0193° and 0.00000024° for the tilting direction. The total errors and the root mean square error of the No. 2 optical pickup are, respectively, 78.64 and 0.0098 μm for the focusing direction, 67.67 and 0.0085 μm for the tracking direction, and 0.0618° and 0.00000077° for the tilting direction. The root mean square error of No. 1 and 2 optical pickups are both smaller than 0.1 μm, showing the satisfactory performance of the designed fuzzy controller equipped with tuning from the genetic algorithm.

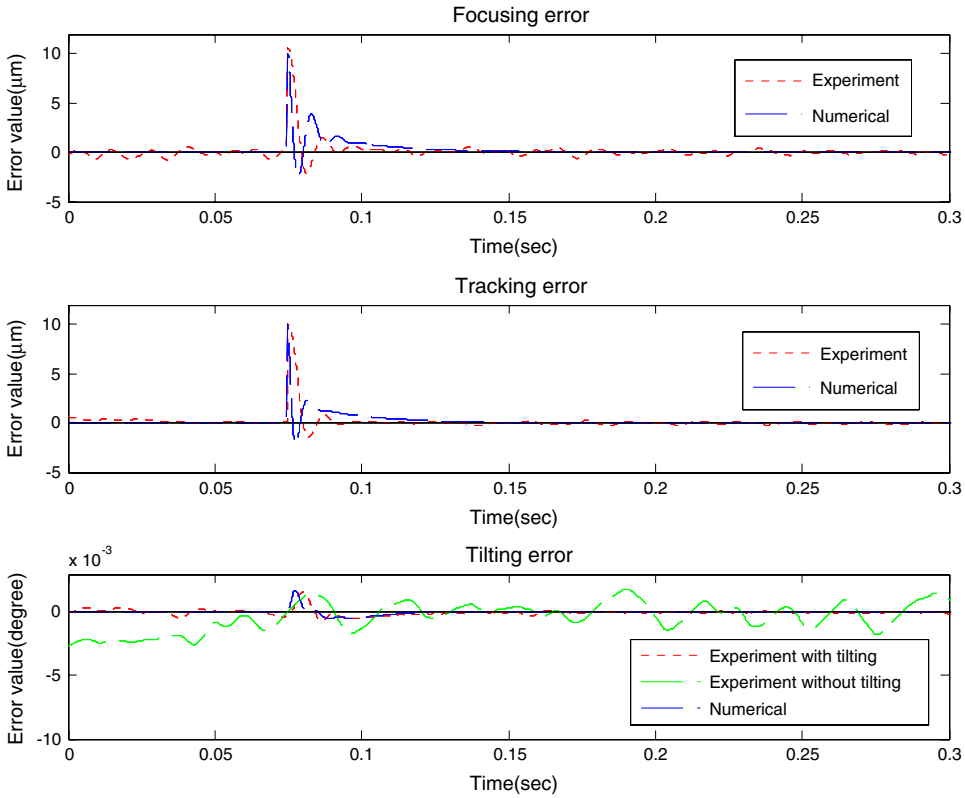

Fig. 25 The position error by the fuzzy double-lead controller with a genetic algorithm

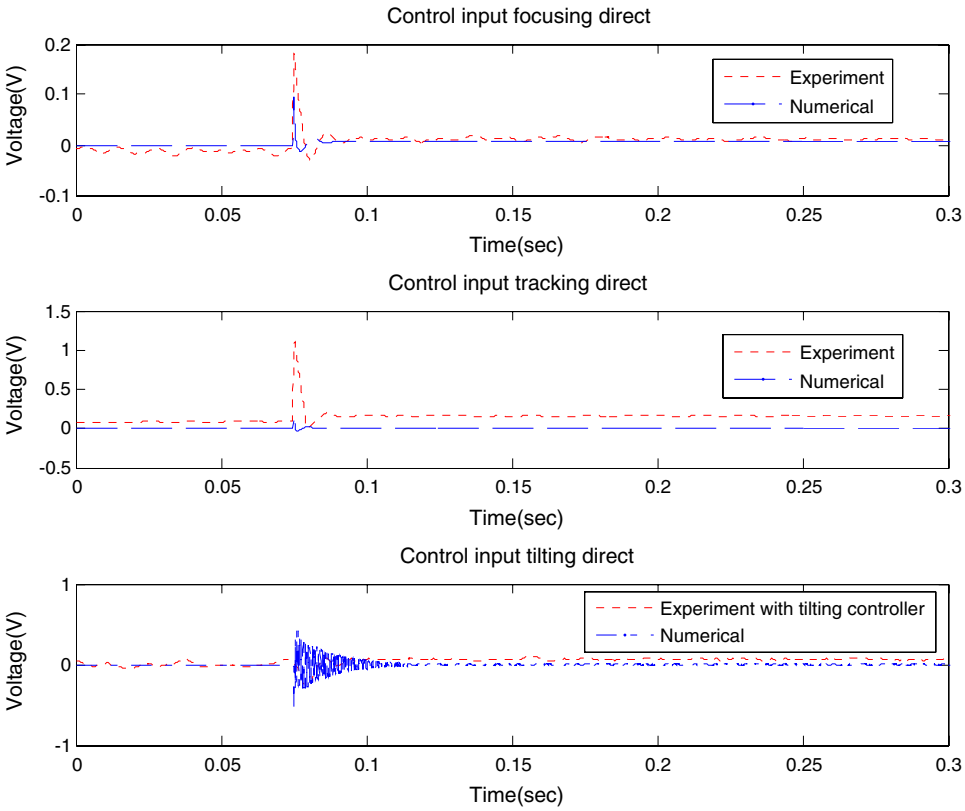

Fig. 26 The control effort by the fuzzy double-lead controller with a genetic algorithm

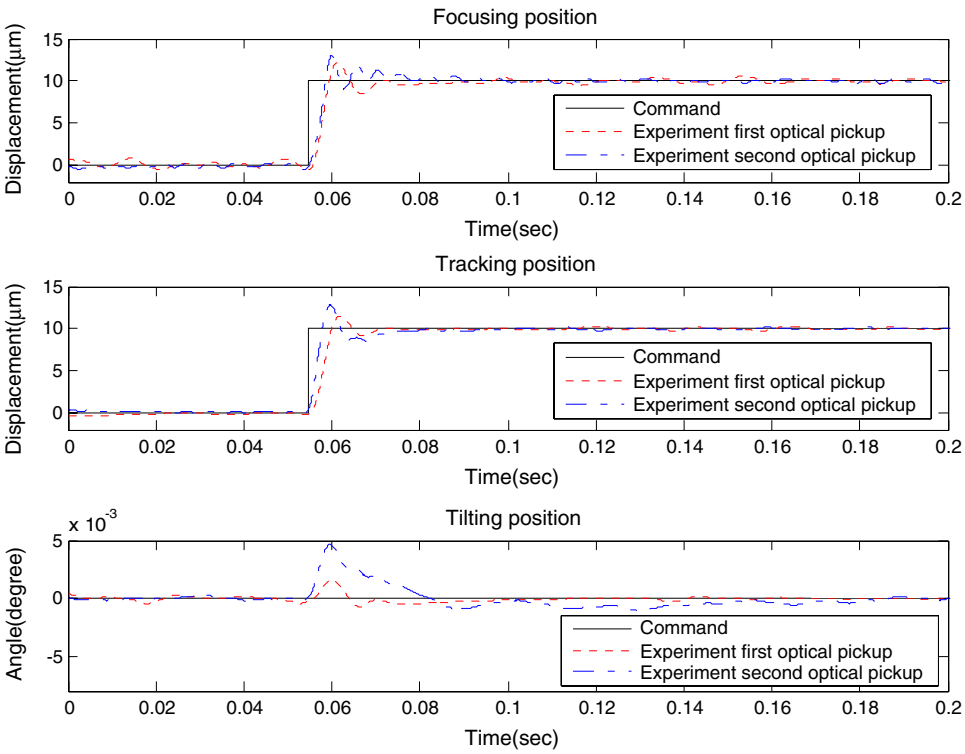

Fig. 27 Experimental results of the the fuzzy double-lead controller with a genetic algorithm in two different three-axis optical pickups

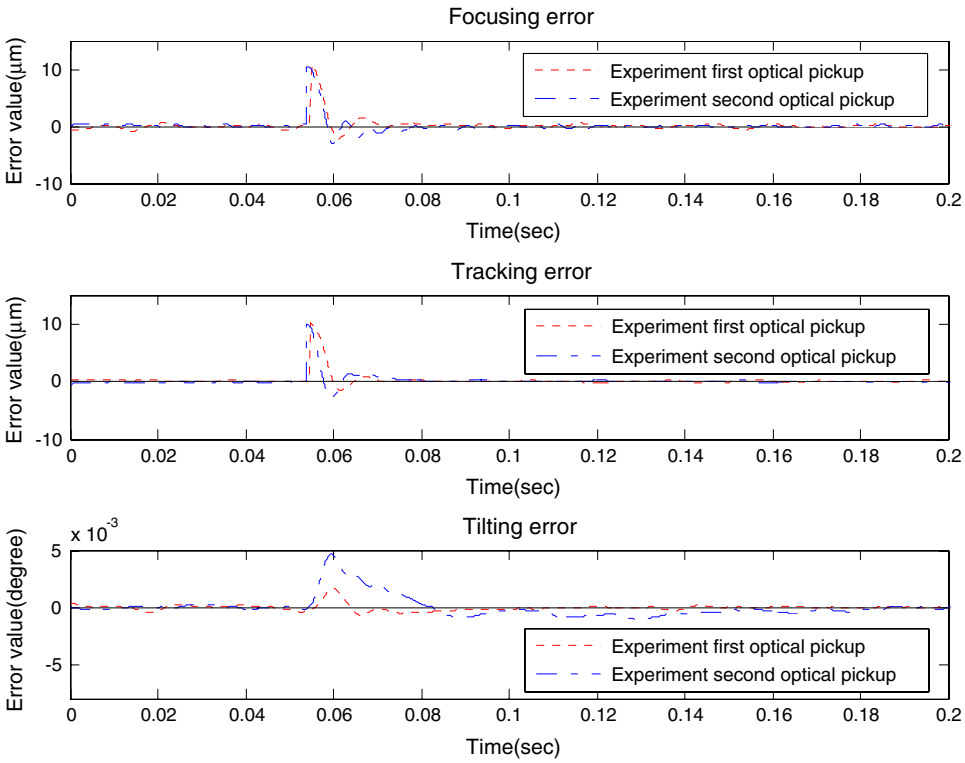

Fig. 28 Experimental position error of the fuzzy double-lead controller with a genetic algorithm in two different three-axis optical pickups

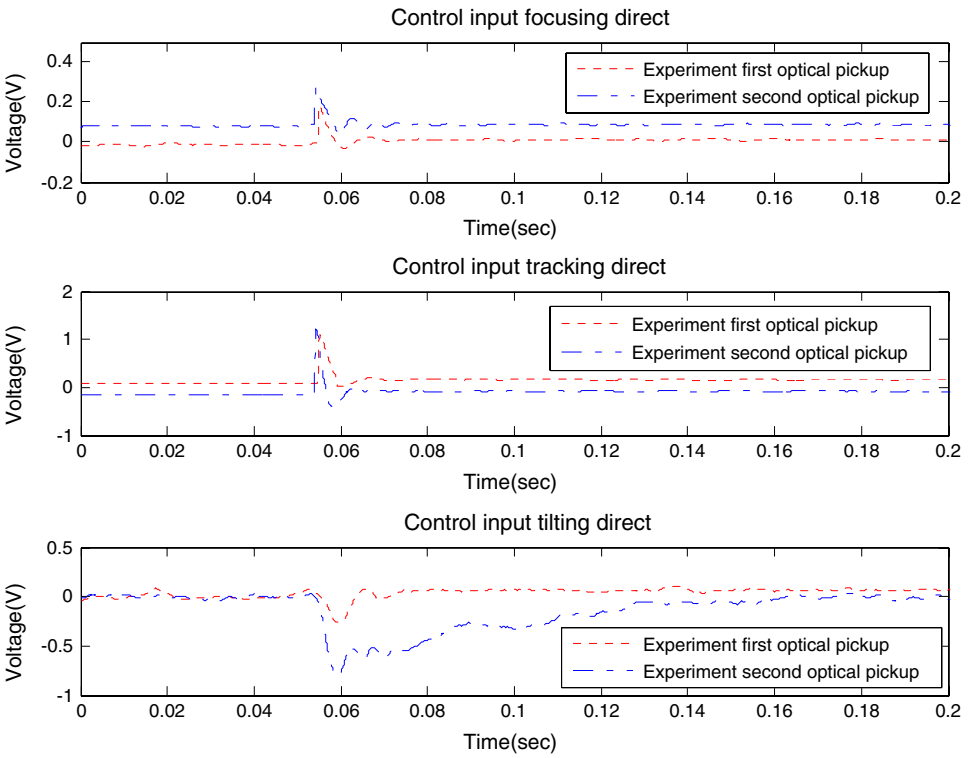

Fig. 29 Experimental control effort of the fuzzy double-lead controller with a genetic algorithm in two different three-axis optical pickups

5 Conclusion

In order to overcome the model uncertainty of the pickups caused by manufacturing tolerance and the coupling between three different DOFs of the three-axis pickup for rendering desired precision data-reading, the auto-tuning algorithm based on the fuzzy double-lead controller assisted by a genetic algorithm is proposed in

this study. The conclusive remarks are summarized as follows:

1. The design process of the auto-tuning algorithm has already been developed successfully. According to the numerical and experimental results, the focusing and tracking of the four-wire type optical pickup can be positioned at 10 μm and the tilting can be controlled to almost 0°.
2. As experimental result shows, the application of auto-tuning algorithm overcomes the couplings among three different DOFs of the three-axis pickup to render precise positioning successfully.
3. In order to attain better performance of the proposed fuzzy double-lead controller, the genetic algorithm is adopted to search optimum membership functions for the fuzzy logic controller was verified by experiments. Shorter settling time and less overshoot of experimental responses are presented.

Acknowledgment The authors are greatly indebted to the National Science Council of ROC for the supports via the research contracts in nos. of NSC 96-2622-E-009-010-CC3 and NSC 97-2221-E-009-057-MY3.

References

Akgül M, Morgül Ö (1997) Fuzzy controller design for parametric controllers. In: Proceedings of the 1997 IEEE international symposium on intelligent control, pp 67–72

Chao PCP, Huang JS, Lai CL (2003) Nonlinear dynamic analysis and actuation strategy for a three-DOF four-wire type optical pickup. Sens Actuator A Phys 105:171–182

Choi IH, Hong SN, Suh MS, Son DH, Kim YL, Park KW, Kim JY (2001) 3-axis actuator in slim optical pick-up for disc tilt compensation. In: Proceedings optical storage topical meeting, pp 178–180

Fan KC, Lin CY, Shyu LH (2000) Development of a low-cost focusing probe measurement. Meas Sci Technol 11:1–7

Fan KC, Lin CY, Shyu LH (2001) Development of a low-cost autofocusing probe measurement. Meas Sci Technol 12:2137–2146

He N, Jia W, Yu D, Huang L, Gong M (2004) A novel type of 3-axis lens actuator with tilt compensation for high-density optical disc system. Sens Actuator A Phys 115:126–132

Hong HP, Park SJ, Han SJ, Cho KY, Lim YC, Park JK, Kim TG (1992) A design of auto-tuning PID controller using fuzzy logic. In: Proceedings of the 1992 international conference on industrial electronics, vol 2, pp 971–976

Hsu YP, Tsai CC (1996) Autotuning for fuzzy-PI control using genetic algorithm. In: Proceedings of the 1996 IEEE IECON 22nd international conference on industrial electronics, vol 1, pp 602–607

Hwang WR, Thompson WE (1994) Design of intelligent fuzzy logic controllers using genetic algorithms. In: Proceedings of the third IEEE conference on fuzzy systems , vol 2, pp 1383–1388

Kang JY, Yoon MG (1998) Robust control of an active tilting actuator for high-density optical disk. In: Proceedings of the American control conference , vol 2, pp 861–865

Katayama R, Meguro S, Komatsu Y, Yamanaka Y (2001) Radial and tangential tilt detection for rewritable optical disks. Jpn J Appl Phys 40(3B):1684–1693

Marchant AB (1990) Optical recording. Addison–Wesley, New York

Meirovitch L (1967) Analytical methods in vibrations. MacMillan, London

Miyano K, Nagara T (2004) A new radial tilt detection method: differential wobble phase detection. In: Proceedings of optical data storage conferences, California, USA (5380), pp 189–196

Nagasato M, Hoshino I (1996) Development of two-axis actuator with small tilt angles for one-piece optical head. Jpn J Appl Phys 1(35):392–397

Rosmalen GV (1987) A floating lens actuator. In: Proceedings of international symposium on optical memory

Visioli A (1999) Fuzzy logic based set-point weight tuning of PID controllers. IEEE Trans Syst Man Cybern A 29(6):587–592

Yamada S, Nishiwaki S, Nakamura A, Ishida T, Yamaguchi H (2000) Track center servo and radial tilt servo system for digital versatile rewritable disc (DVD-RAM). Jpn J Appl Phys 39(12B):867–870

Yamasaki F, Arai A, Alkoh H (2006) Radial tilt detection using push-pull signals. Jpn J Appl Phys 45(2B):1158–1161

Zhang J, Cai L (1997) An autofocusing measurement system with a piezoelectric translator. IEEE ASME Trans Mechatron 2:213–216